Caltech Core-Collapse Project (CCCP) observations of type IIn supernovae: typical properties and implications for their progenitor stars

Michael Kiewe, Avishay Gal-Yam, Iair Arcavi

Benoziyo Center for Astrophysics, Faculty of Physics, The Weizmann Institute of Science, Rehovot 76100, Israel

avishay.gal-yam@weizmann.ac.il

and

Douglas C. Leonard, J. Emilio Enriquez

Department of Astronomy, San Diego State University, San Diego, CA 92182.

S. Bradley Cenko

Department of Astronomy, University of California, Berkeley, CA 94720-3411.

Derek B. Fox

Department of Astronomy and Astrophysics, 525 Davey Laboratory, Pennsylvania State University, University Park, PA 16802.

Dae-Sik Moon

Department of Astronomy and Astrophysics, University of Toronto, Toronto, ON M5S 3H4, Canada

David J. Sand, Alicia M. Soderberg

Harvard-Smithsonian Center for Astrophysics, 60 Garden Street, Cambridge MA 02138

(the CCCP)

ABSTRACT

Type IIn Supernovae (SNe IIn) are rare events, constituting only a few percent of all core-collapse SNe, and the current sample of well observed SNe IIn is small. Here, we study the four SNe IIn observed by the Caltech Core-Collapse Project (CCCP). The CCCP SN sample is unbiased to the extent that object

selection was not influenced by target SN properties. Therefore, these events are representative of the observed population of SNe IIn. We find that a narrow P-Cygni profile in the hydrogen Balmer lines appears to be a ubiquitous feature of SNe IIn. Our light curves show a relatively long rise time (> 20 days) followed by a slow decline stage (0.01 to 0.15 mag day^{-1}), and a typical V-band peak magnitude of $M_V = -18.4 \pm 1.0$ mag. We measure the progenitor star wind velocities ($600 - 1400$ km s^{-1}) for the SNe in our sample and derive pre-explosion mass loss rates ($0.026 - 0.12$ M$_\odot$ y^{-1}). We compile similar data for SNe IIn from the literature, and discuss our results in the context of this larger sample. Our results indicate that typical SNe IIn arise from progenitor stars that undergo LBV-like mass-loss shortly before they explode.

Subject headings: supernovae: general

1. Introduction

For many decades it has been known that hydrogen-rich type II supernovae (SNe; Minkowski 1941; see Filippenko 1997 for a review on SN spectroscopic classification) arise from the gravitational core-collapse of massive stars (e.g., Arnett et al. 1989; Smartt 2009). Schlegel (1990) recognized that a small subset of SNe II show narrow emission lines, and proposed that they constituted a separate subclass (SNe IIn). It has been suggested that the narrow emission lines of SN IIn originate from photoionized dense wind surrounding the exploding stars (Chugai 1991). It was later noticed that some SNe IIn (e.g., SN 1988Z) show, in addition to a narrow unresolved Hα emission component ($\Delta v < 200\,\mathrm{km\,s^{-1}}$) also an intermediate component ($\Delta v \sim 10^3\,\mathrm{km\,s^{-1}}$; Stathakis & Sadler 1991). This component has been interpreted as a result of radiative shocks in dense wind clouds (Chugai & Danziger 1994), though other explanations have been suggested (Chugai 2001; Dessart et al. 2009).

Over the years, a specific model has emerged, which describes the properties of SNe IIn as a result from a combination of emission from several physically distinct regions (see Smith et al. 2008 for a recent description). In brief, it is assumed that the SN ejecta interact with a massive slower wind blown by the progenitor star, launching a pair of forward and reverse shocks. The blast wave is decelerated by the interaction from its initial velocity, and a dense shell traveling approximately at the shock velocity is formed. Initially, this dense shell is optically thick, and obscures the actual electron-scattering photosphere of the supernova which lies interior to the shock. At this stage (which can, in principle, have a duration of years), the optical spectrum is dominated by a blue continuum from the shocked material, superposed with emission lines. The emission lines often have a complex profile, including

a narrow component from the photoionized, outer unshocked wind, and an intermediate-width component from the shocked dense shell. Later on, as the interaction weakens, the shocked region may become optically thin and the underlying supernova photosphere (with its high-velocity absorption-dominated spectrum) may emerge (e.g., Gal-Yam & Leonard 2009). Applying such a model, one can extract the physical properties of the progenitor star (in particular, its mass-loss rate) from the observations (e.g., Salamanca et al. 1998, Gal-Yam & Leonard 2009). Previously derived values (summarized in Table 5) show progenitor wind velocities of $50-1000\,\mathrm{km\,s^{-1}}$ and mass loss rates that range between $10^{-4}-0.3\,\mathrm{M_\odot\,y^{-1}}$. These are consistent with a variety of possible massive progenitors, from red supergiant stars (RSGs; typical wind velocities of tens of $\mathrm{km\,s^{-1}}$, e.g., Smith et al. 2007) and small mass-loss rates ($\lesssim 10^{-5}\,\mathrm{M_\odot\,y^{-1}}$), to stripped Wolf-Rayet (W-R) stars with fast (thousands of $\mathrm{km\,s^{-1}}$) and more massive winds ($\sim 10^{-4}\,\mathrm{M_\odot\,y^{-1}}$), up to Luminous Blue Variable stars (LBVs) which have the most extreme mass-loss rates (up to $\sim 10^{-2}\,\mathrm{M_\odot\,y^{-1}}$) and intermediate-velocity winds (a few hundreds of $\mathrm{km\,s^{-1}}$; e.g., Humphreys & Davidson 1994).

The connection between SNe IIn and LBVs was brought into focus by studies of SN 2005gl. Gal-Yam et al. (2007a) analyzed pre-explosion images of this SN IIn, and detected a possible progenitor, whose extreme luminosity ($\mathrm{L}_V > 10^6\,\mathrm{L_\odot}$) suggested an LBV identification (the only stars of comparable properties known in our galaxy are LBVs). Gal-Yam et al. (2007) also noted that the relative rarity and spectral appearance of SNe IIn could be naturally explained by an origin in very massive LBVs (with $\mathrm{M} \gtrsim 80\,\mathrm{M_\odot}$). Gal-Yam & Leonard (2009) subsequently presented post-explosion HST data of this event that showed the putative progenitor of SN 2005gl had disappeared, providing strong evidence that this SN IIn had indeed originated from a single massive LBV-analog. These authors also analyzed the spectra of SN 2005gl and showed that the derived mass-loss rate was consistent with that of eruptive LBVs (e.g., P-Cygni during its sixteenth century eruption). Other work on additional SNe supports the SN IIn-LBV connection (e.g., Smith et al. 2007; Trundle et al. 2008).

It remains an open question how general the SN IIn-LBV connection is, i.e., are most or all SNe IIn related to LBVs, or stars with similar properties? A literature-based study of this question is weakened due to the fact that the sample of SNe IIn published thus far may be highly biased, due to the tendency of authors to preferentially publish extreme or unusual events (this is evident for many of the objects, as summarized in section § 4 and Table 5).

Here we present and analyze four SNe IIn observed by the Caltech Core-Collapse Project (CCCP; Gal-Yam et al. 2007b; Gal-Yam et al. 2010, in preparation). The CCCP supernova sample is unbiased in the sense that essentially every young core-collapse SN that was ob-

servable from Palomar Observatory during the project was followed-up, without preference. Thus, the objects included within the CCCP should fairly represent the population of observed SNe IIn. Typical wind velocities and mass-loss rates can therefore be derived, which may help constrain the properties of the progenitor stars. We organize the paper as follows. In § 2 we present our observations, and derive physical parameters for the sample in § 3. We present an exhaustive literature review of SNe IIn in § 4, and discuss our results in § 5. We conclude with a summary in § 6.

2. Observations

The observations reported here were taken as part of the CCCP (Gal-Yam et al. 2007b, Gal-Yam et al. 2010 in preparation). The CCCP obtained photometric (optical and near-IR) and spectroscopic observations of 50 core-collapse SNe. The program is designed to provide a fair sample of core-collapse events, with well-defined selection criteria and uniform, high-quality optical/IR observations. One of the goals of the CCCP is to characterize the little-studied properties of core-collapse SNe as a population. 4 SNe IIn are included in the CCCP SN sample.

2.1. Discovery

SN 2005bx was discovered by Rich (2005) on April 27, 2005, and was absent on April 11, 2005. It was thus discovered within 16 days of explosion. The host galaxy, MCG +12-13-19 is at z=0.031218 (NED[1]). Bonnaud et al. (2005) identified SN 2005bx as an SN IIn based on a spectrum taken on May 1, 2005; our earlier spectrum from April 30 (Gal-Yam et al. 2005) confirms this identification.

Pugh & Li (2005) reported the discovery of SN 2005cl by LOSS (Filippenko et al. 2001). The SN was detected on June 2 (marginal) and June 12, 2005, and was absent on May 23, 2005, so it too was discovered rather young. The host galaxy MCG -01-53-20 is at z=0.025878 (NED). A spectrum taken by Modjaz et al. (2005a) on June 13, 2005 demonstrates that SN 2005cl was a SN IIn.

Lee et al. (2005) reported the LOSS (Filippenko et al. 2001) discovery of SN 2005cp on June 20, 2005. Spectroscopy by Modjaz et al. (2005b) on June 30, 2005 indicated a young age and IIn classification. The host galaxy, UGC 12886, is at z=0.022115 (NED). Our light

[1]see http://nedwww.ipac.caltech.edu

curve confirms that this was a young SN found on the rise (see Fig. 3 below).

SN 2005db was discovered by Monard (2005) on July 19, 2005, and was absent on July 2, 2005, so it was discovered rather early. The host galaxy, NGC 214, is at z=0.015124 (NED). Blanc et al. (2005) identified this event as a type IIn based on a spectrum taken on July 20, 2005. Our light curve confirms that this was a young SN found on the rise (Fig. 4).

2.2. Photometry

We obtained optical photometry with the 1.5 m robotic telescope at the Palomar Observatory (P60; Cenko et al. 2006) using a 2048 x 2048 pixel CCD in the Johnson-Cousins $BVRI$ bands. All images were pipeline-reduced by the automated P60 software, applying standard bias- and flatfield-correction, as well as an astrometric solution.

We derived light curves using the image-subtraction-based photometry routine mkdifflc (Gal-Yam et al. 2004), implemented within IRAF[2]. This pipeline performs image registration followed by reference image subtraction using the Common PSF Method (CPM; Gal-Yam et al. 2008), relative calibration with respect to local standards, and error calculation.

Field calibration was carried out relative to stars near the SN location with absolute photometry obtained in two ways. In the fields of SN 2005cl and SN 2005db, SDSS cataloged gri magnitudes of nearby stars were transformed to the $BVRI$ Vega-based system using the equations of Jordi et al (2005). The fields of SN 2005bx and SN 2005cp are not within the SDSS footprint. For those we obtained standard photometric calibration using Landolt standards taken by the P60 on photometric nights. Additional discussion of photometric calibration, as well as finding charts for the nearby calibration stars used for the 4 SN fields in this work, are given in the appendix.

Photometry of all SNe was corrected for Galactic extinction (Schlegel, Finkbeiner & Davis 1998; via NED). The final light curves were also corrected for extinction in the host galaxy by first estimating using the IRAF *splot* routine the equivalent width (EW) of the Na I D absorption feature in our spectra and then calculating the excess color E(B-V) from the EW using the formula of Turatto et al. (2003). In two cases (SN 2005cl and SN 2005bx) an apparently unrelated noise fluctuation falls close to the Na D feature in our best spectra. We also calculate an upper limit on the extinction assuming this apparent noise feature is

[2]IRAF (Image Reduction and Analysis Facility) is distributed by the National Optical Astronomy Observatories, which are operated by AURA, Inc., under cooperative agreement with the National Science Foundation.

due entirely to Na D absorption. We view this upper limit as very conservative. Therefore, we corrected the light curves shown for the most likely estimate reported in the table. In the mass loss calculations below we adopt the average between the likely estimate and upper limit as our extinction value, and propagate the range bracketed between these values in the mass loss error calculations. The adopted extinctions are given in Table 1.

Late images (mid-end November 2005) of SN 2005db do not show signal from the SN. An upper limit on its luminosity was therefore calculated by introducing artificial point sources of decreasing flux at the SN location and using the SEXTRACTOR software (Bertin & Arnouts 1996) to determine when the artificial object was detected at 3σ confidence. These values are adopted as the reported upper limits.

The photometric light curves of all 4 SNe are presented in Figures 1 – 4. The errors include photometric errors due to non-perfect image subtraction and Poisson errors (derived by *mkdifflc*), extinction uncertainty errors, zeropoint calibration errors, and distance modulus errors taken from NED, which usually dominate the errors in peak absolute magnitudes (≈ 0.15 mag). We determined peak magnitudes and dates from low-order polynomial fits to the data (example fits to the R-band data are presented). Rise times were estimated using our data combined with reported non-detections, assumed to have been obtained in bands closely matching the R-band (section 2.1). Post-peak decay slopes were determined from linear fits. SN 2005cl showed a clear break in the decline rate, so a broken linear fit was used. The BVRI peak values, dates, rise times and decline rates are listed in table 2.

	SN 2005bx	SN 2005cl	SN 2005cp	SN 2005db
E(B-V)$_{Galactic}$ [mag]	0.019	0.073	0.031	0.036
Na I D EW (likely)[Ang]	0.67	0.73	0.12	0.58
E(B-V)$_{Host}$ [mag]	0.3	0.33	0.02	0.26
Na I D EW (upper limit)[Ang]	1.09	0.95		
E(B-V)$_{Host,limit}$ [mag]	0.52	0.45		

Table 1: Adopted extinction values

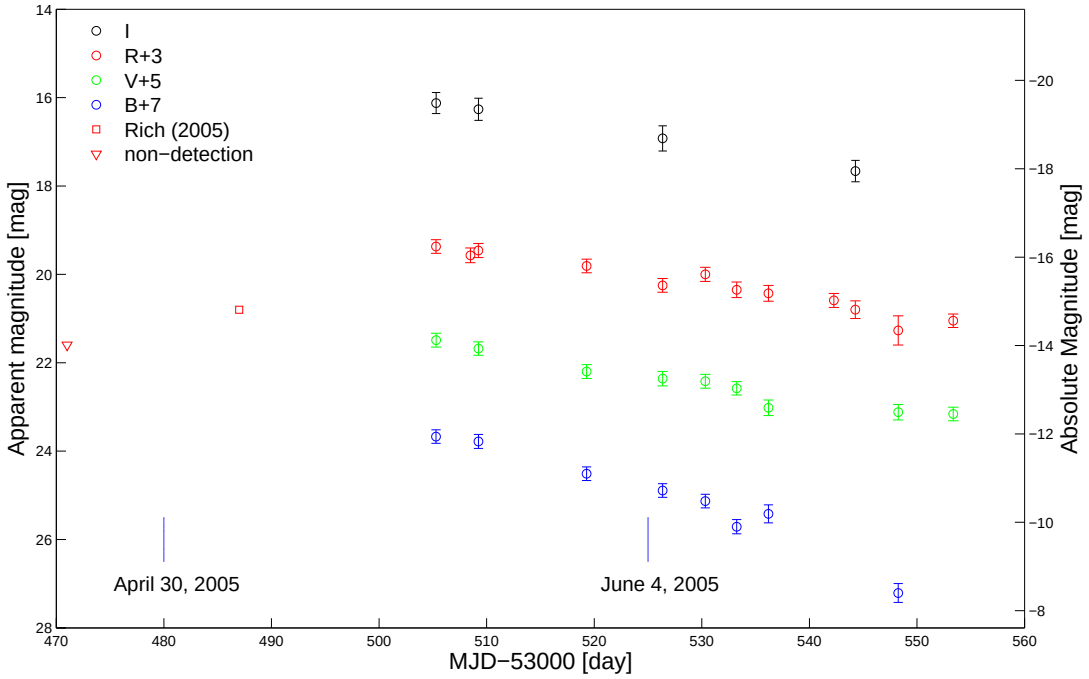

Fig. 1.— $BVRI$ light curves of SN 2005bx. Discovery magnitude and previous non-detection from Rich (2005) are plotted, on an R-band grid. Our follow-up campaign missed the peak (values given in table 2 are for our first, brightest point). The VRI bands have a similar decline rate, while the B-band declines approximately twice as fast. The dashed blue lines mark the spectroscopic observation epochs of SN 2005bx.

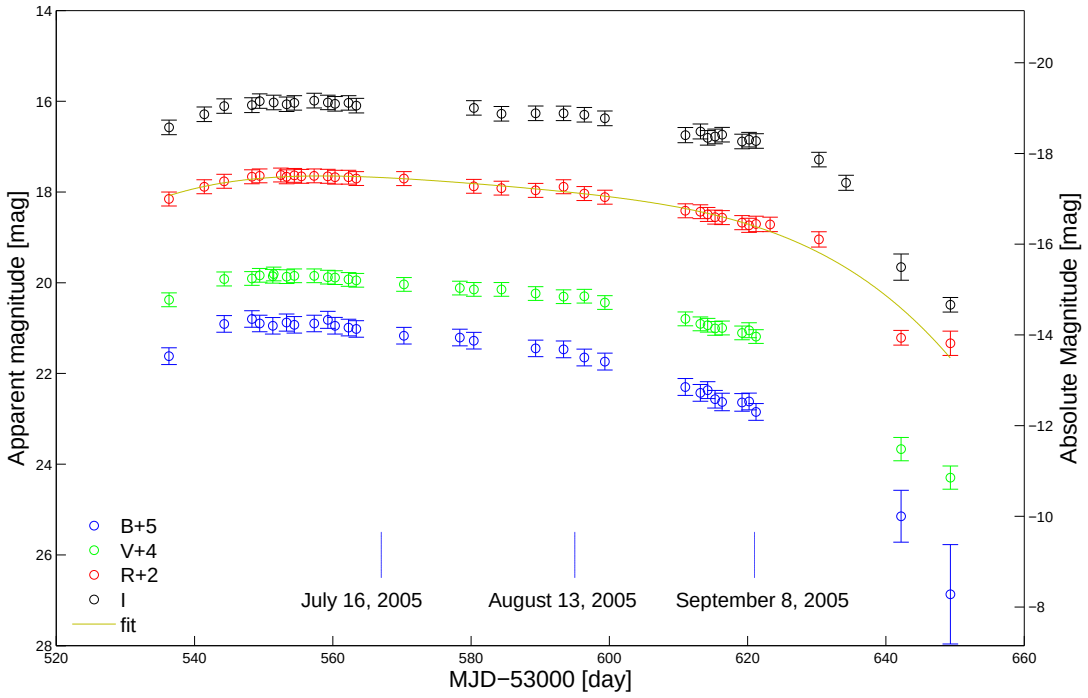

Fig. 2.— $BVRI$ light curves of SN 2005cl. Our data trace a slow rise to peak magnitude, followed by a slow decay, with an obvious break to a steeper decline around MJD 53625 day. The blue vertical lines mark the spectroscopic observation epochs of SN 2005cl.

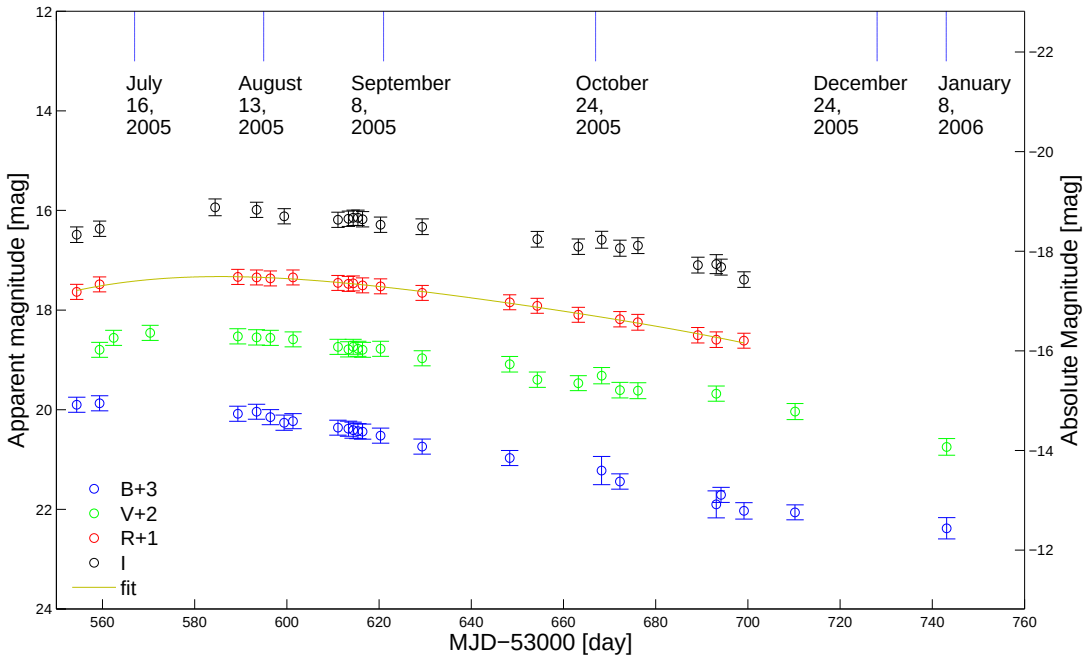

Fig. 3.— $BVRI$ light curves of SN 2005cp. The SN exhibits a slow rise to peak, followed by an extended decline stage of constant slope. The blue vertical lines mark the spectroscopic observation epochs of SN 2005cp.

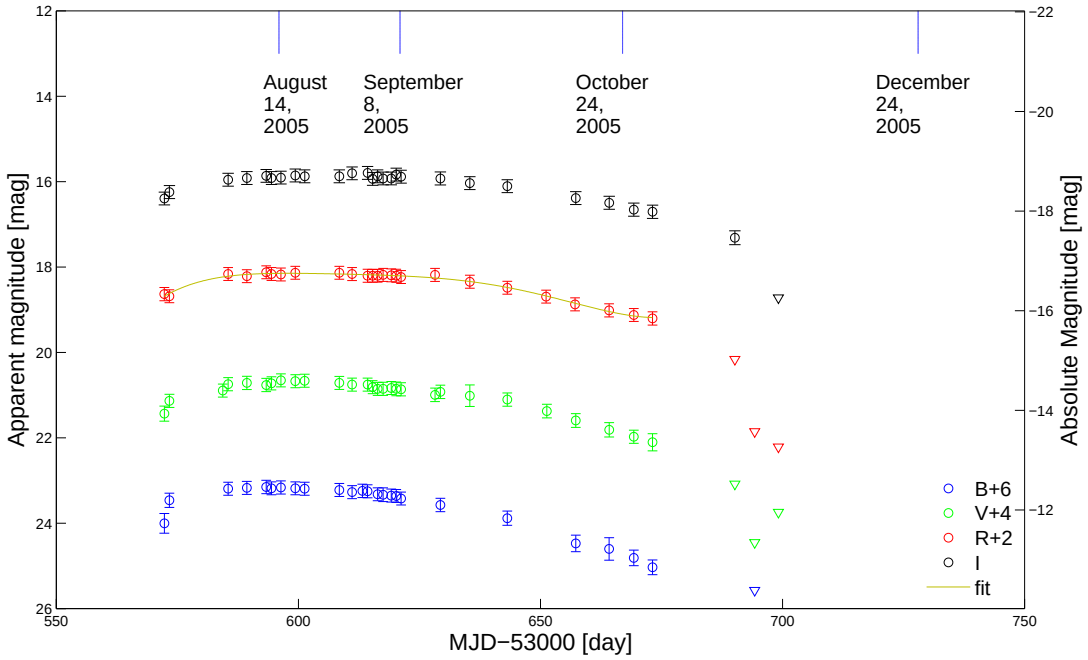

Fig. 4.— $BVRI$ light curves of SN 2005db. The SN has an initially rapid rise followed by a broad peak. Following the peak, there is a period of 30-40 days in which the SN magnitude is almost constant. This is followed by a slow decline which is faster in bluer bands, that eventually turns into a sharp drop in the SN luminosity, traced by the upper limits marked by downward-facing triangles. This magnitude drop can be evaluated in the VRI bands to be between 1-2 mag within 4-9 days. This sharp drop in magnitude may be indicative of a CSM distribution with a sharp cutoff, leading to an abrupt luminosity decrease as the ejecta emerge from the previously ejected mass shell and the interaction effectively stops. The dashed blue lines mark the spectroscopic observation epochs of SN 2005db.

SN 2005bx					
Band	Peak magnitude [mag]	MJD [day]	Rise time [day]	Initial slope [mag/day]	Final slope [mag/day]
B	-18.94 ± 0.15	53505		0.077 ± 0.019	
V	-19.12 ± 0.15	53505		0.036 ± 0.008	
R	-19.24 ± 0.15	53505	< 34	0.037 ± 0.006	
I	-19.49 ± 0.15	53505		0.040 ± 0.002	
SN 2005cl					
B	-19.28 ± 0.15	53553		0.026 ± 0.003	0.14 ± 0.06
V	-19.32 ± 0.15	53554		0.018 ± 0.002	0.11 ± 0.07
R	-19.50 ± 0.15	53556	$14 - 34$	0.016 ± 0.002	0.11 ± 0.09
I	-19.14 ± 0.15	53557		0.012 ± 0.002	0.18 ± 0.07
SN 2005cp					
B	-17.98 ± 0.15	53565		0.016 ± 0.001	
V	-18.17 ± 0.15	53581		0.014 ± 0.001	
R	-18.48 ± 0.15	53584	> 32	0.012 ± 0.001	
I	-18.85 ± 0.15	53586		0.011 ± 0.001	
SN 2005db					
B	-16.89 ± 0.15	53587		0.028 ± 0.002	
V	-17.32 ± 0.15	53598		0.020 ± 0.002	
R	-17.87 ± 0.15	53597	$10 - 27$	0.011 ± 0.001	
I	-18.17 ± 0.15	53607		0.021 ± 0.004	

Table 2: Photometric light curve parameters for SNe 2005bx, 2005cl, 2005cp, 2005db.

2.3. Spectroscopy

Spectroscopic observations were carried out using the double beam spectrograph (DBSP; Oke & Gunn 1982) mounted on the 5 m Hale telescope at the Palomar Observatory. We used the D55 dichroic, with 600/158 line/mm grisms in the blue/red sides, respectively. We obtained a continuous spectrum covering the wavelength range 3400 – 9400 Å. The instrumental resolution was 4.88 Å per pixel in the red and 1.08 Å per pixel in the blue. The typical exposure time was between 10 and 30 minutes, see table 3 for more details.

Spectroscopic reduction was performed using the CCCP spectroscopic pipeline, which is based on IRAF and IDL scripts as described, e.g., in Matheson et al. (2000), and Gal-Yam et al. (2007). In brief, to derive the total-flux spectrum, we extracted the one dimensional sky-subtracted spectra optimally (Horne 1986) in the usual manner. The spectra were then wavelength and flux calibrated, corrected for continuum atmospheric extinction and telluric absorption bands (Wade & Horne 1988; Bessell 1999; Matheson et al. 2000).

Our resulting spectroscopic time series are presented in figures 5-11. We discuss each object separately below.

Supernova	UT Date	exposure time [sec]	Observers	Comments
2005bx	Apr. 30, 2005	900	Sand & Cenko	-
	June 4, 2005	1200	Gal-Yam & Sand	-
	July 16, 2005	1200	Gal-Yam & Sharon	slightly cloudy
2005cl	July 16, 2005	600	Gal-Yam & Sharon	-
	Aug. 13, 2005	1800	Cenko	-
	Sep. 8, 2005	1800	Leonard	clear sky, poor seeing
2005cp	July 16, 2005	600	Gal-Yam & Sharon	clear sky
	Aug. 13, 2005	1800	Cenko	-
	Sep. 8, 2005	1800	Leonard	clear sky, poor seeing
	Oct. 24, 2005	1800	Gal-Yam	-
	Dec. 24, 2005	1800	Sand	-
	Jan. 8, 2006	1800	Cenko & Ballmer	-
	Jan. 20, 2006	1800	Moon	-
2005db	Aug. 14, 2005	1200	Sand	-
	Sep. 8, 2005	900	Leonard	-
	Oct. 24, 2005	900	Gal-Yam	clear
	Dec. 24, 2006	1800	Sand	poor seeing
	Jan. 8, 2006	1800	Cenko & Ballmer	-
	Jan. 20, 2006	1800	Moon	-

Table 3: Log of spectroscopic observations

2.3.1. SN 2005bx

We present our spectroscopy of SN2005bx in Fig. 5. The continuum shape was initially blue, and reddened with time. Except for the Balmer emission lines, there are no other strong features. The intermediate-width component of the Hα line is evident in the first spectrum, which we decompose in Fig. 13 below, and disappears in later spectra. None of our spectra exhibit P-Cygni profiles in the narrow lines.

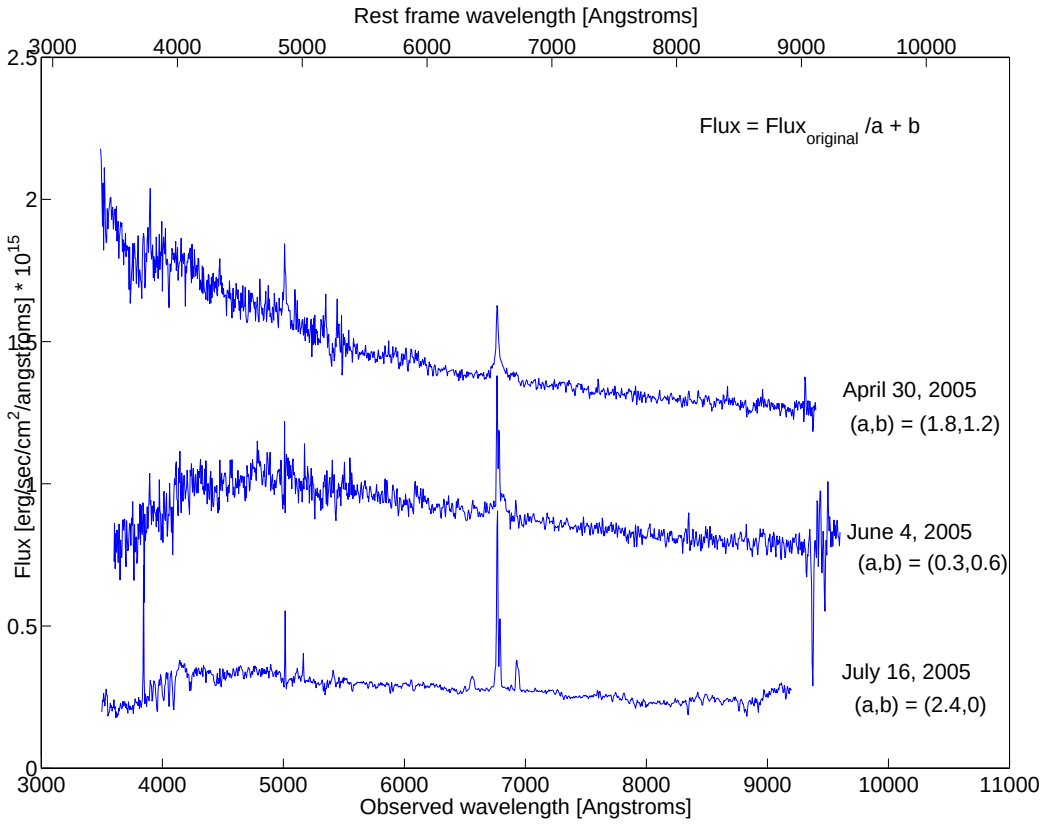

Fig. 5.— Spectral evolution of SN2005bx. The intermediate component evident in the first spectrum fades away in later observations.

2.3.2. SN 2005cl

We present our spectroscopy of SN2005cl in Fig. 6, showing the spectral evolution of the SN. One can see the hallmark of a type IIn SN in the form of narrow hydrogen emission lines with a P-Cygni profile (that indicating the presence of an expanding envelope) in H_α, H_β, H_γ and H_δ. The unshocked wind velocity was calculated from the H_α P-Cygni profile (Fig. 7). In Fig. 14 we present the decomposition of the H_α feature in our first spectrum into different Gaussian components, showing the presence of an intermediate-width component. In later spectra this component is not clearly visible, while the narrow P-Cygni profiles in the Balmer lines persist. The relatively high resolution of our blue spectra reveals that in these later epochs, the continuum "bump" on the blue is actually a pseudo-continuum, and is at least partially resolved into numerous very narrow P-Cygni profiles, mainly of Fe II lines (Fig. 8).

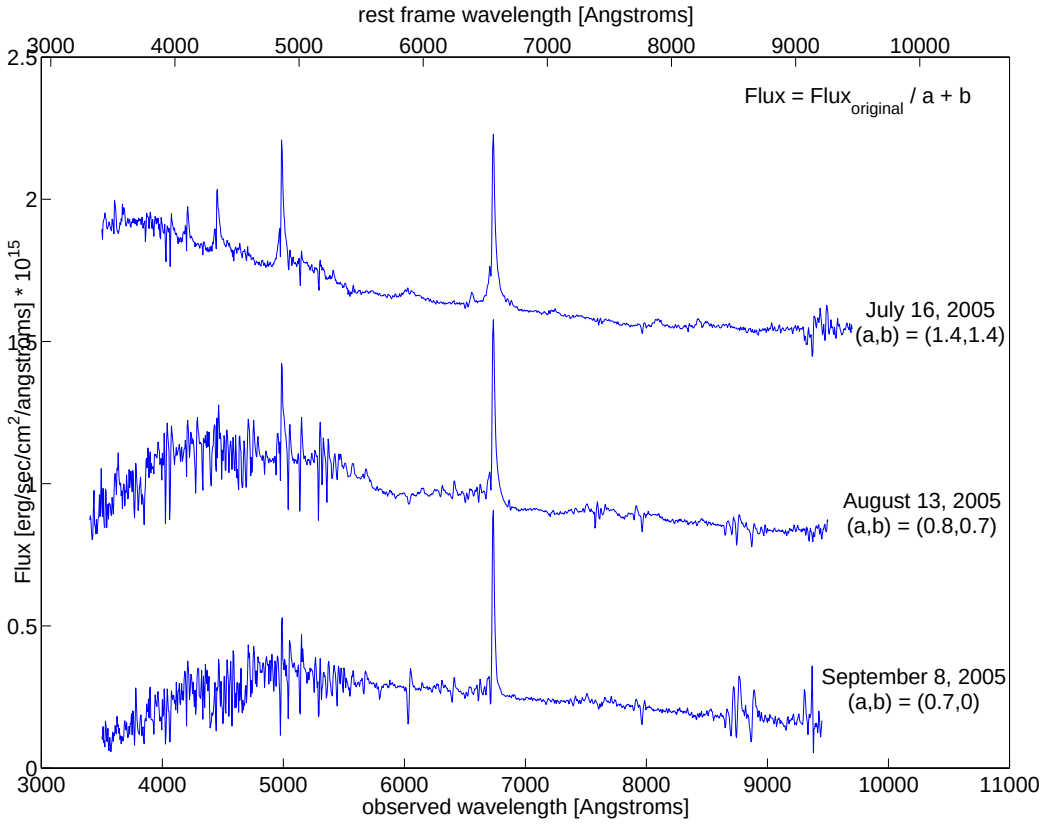

Fig. 6.— Spectral evolution of SN2005cl. One can see that the intermediate component of the Balmer lines fades away in the later observations. Note the narrow P-Cygni profile in the 4 first Balmer lines in the earliest spectrum.

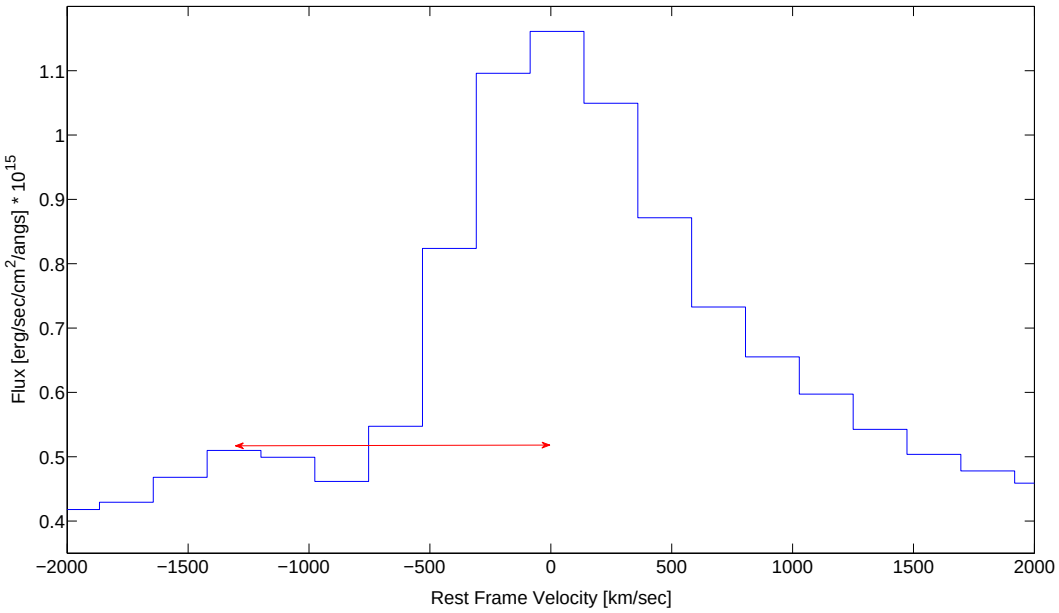

Fig. 7.— The H_α emission line in our first spectrum of SN2005cl shows a clear P-Cygni profile. The red arrow marks the velocity offset of the blue edge of the absorption feature, used to estimate the progenitor wind velocity.

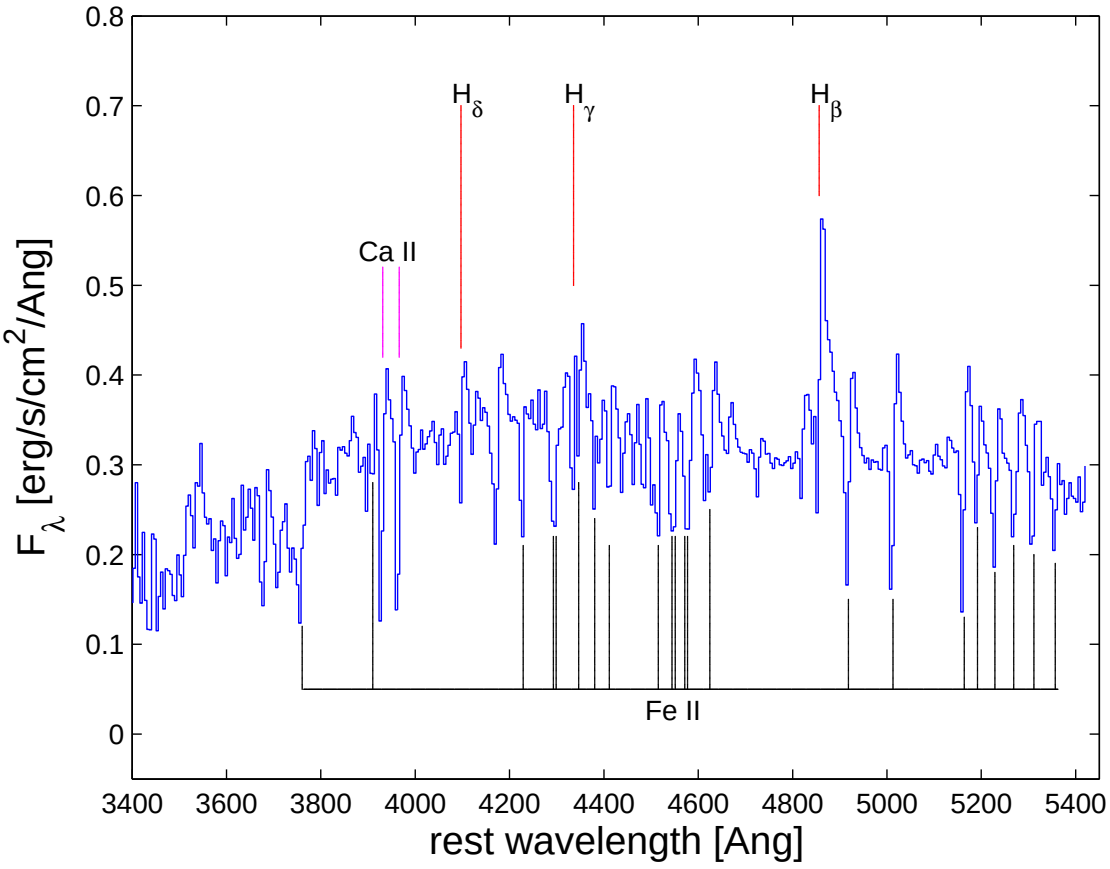

Fig. 8.— A zoomed-in section of the Sep. 8, 2005 spectrum of SN 2005cl. Note that the blue continuum bump is partially resolved into multiple narrow P-Cygni profiles of H, Fe II and Ca II.

2.3.3. SN 2005cp

We present our spectroscopy of SN2005cp in Fig. 6. The first spectrum shows a blue continuum bump (not resolved into individual lines) and prominent Balmer emission lines. In later spectra the blue continuum fades, while SN photospheric features emerge, including a broad base below the strong Balmer emission lines, a broad line with P-Cygni profile blueward of 6000Å which could be He I 5876Å (or Na D), and later on, a broad Ca IR triplet. A strong H_α emission dominates the spectrum at very late times. In Fig. 15, we zoom in on the H_α feature in the August spectrum and extract the unshocked wind velocity from the decomposition of the H_α feature into different Gaussian components. The July and September spectra were analyzed in the same way and provided consistent results. In Fig. 10, we zoom in on the H_α feature in the January 8th spectrum and extract the unshocked wind velocity from the P-Cygni profile.

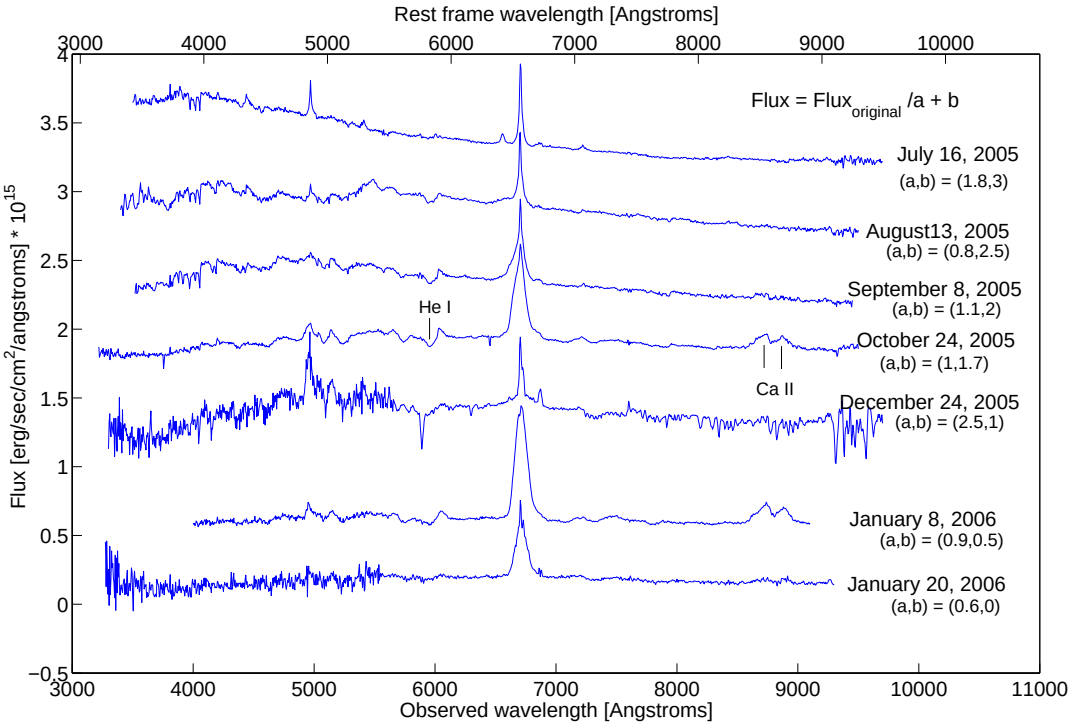

Fig. 9.— Spectral evolution of SN2005cp. Broad, intermediate, and narrow components are prominent in the August 13 spectrum (second from top). The blue continuum in early spectra is not resolved into individual lines, and narrow P-Cygni features appear only in the H_α feature in a late spectrum. A strong H_α emission line dominates the spectrum at late times.

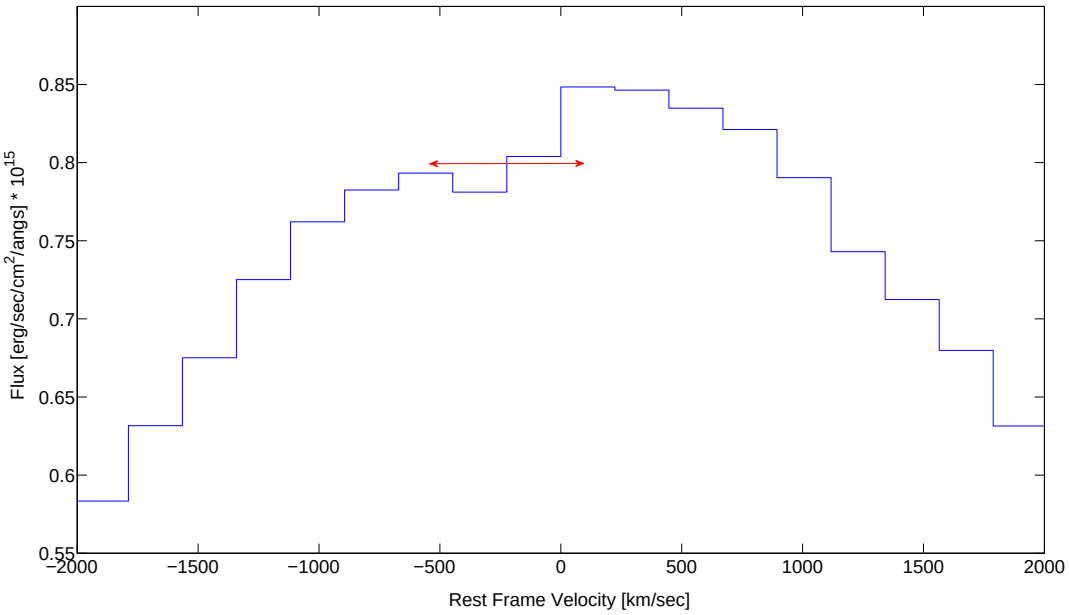

Fig. 10.— The H_α emission line in our January 8 spectrum of SN2005cp shows a clear P-Cygni profile. The red arrow marks the velocity offset of the blue edge of the absorption feature, used to estimate the progenitor wind velocity.

2.3.4. SN 2005db

We present our spectroscopy of SN2005db in Fig. 11. Early spectra have very smooth continua with composite Balmer emission lines clearly showing narrow and intermediate-width components as well as narrow P-Cygni absorption features. Weak He I 5876Å is also seen in the first two spectra. The October spectrum shows developing intermediate-width P-Cygni profiles in the Balmer series, He I, Ca IR triplet and emerging Fe II lines near 5000Å. Later spectra seem dominated by host galaxy emission, in accordance with the light curve (Fig. 4) showing a steep drop in the SN luminosity. In Fig. 16, we zoom in on the H_α feature in the August spectrum and extract the unshocked wind velocity from the decomposition of the H_α feature into different Gaussian components. In Fig. 12, we zoom in on the H_β feature in the September spectrum and extract the unshocked wind velocity from the P-Cygni profile. The P-Cygni profile in the H_β feature in the October spectrum was also analyzed and provides consistent results.

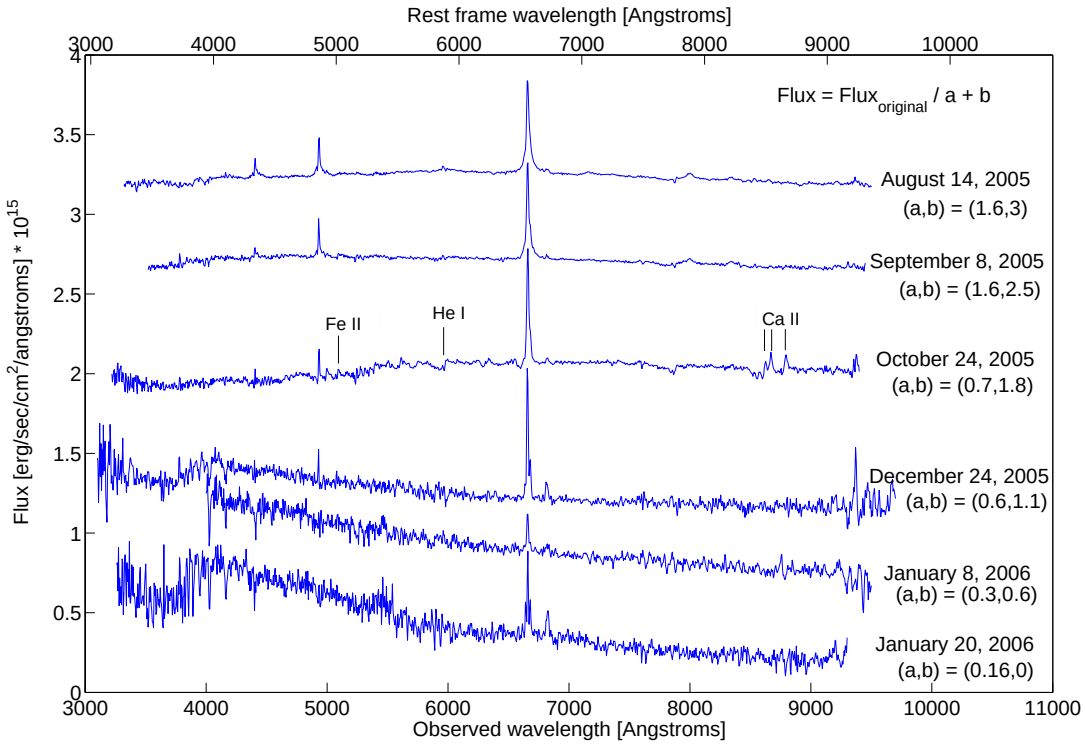

Fig. 11.— Spectral evolution of SN2005db. Composite profiles of the Balmer lines are evident, with narrow P-Cygni profiles. The October spectrum shows emerging intermediate-width P-Cygni profiles of Fe II, He I and the Ca II IR triplet. The last 3 spectra appear to be dominated by the host galaxy light, similar to a starburst template spectrum from Kinney (1996).

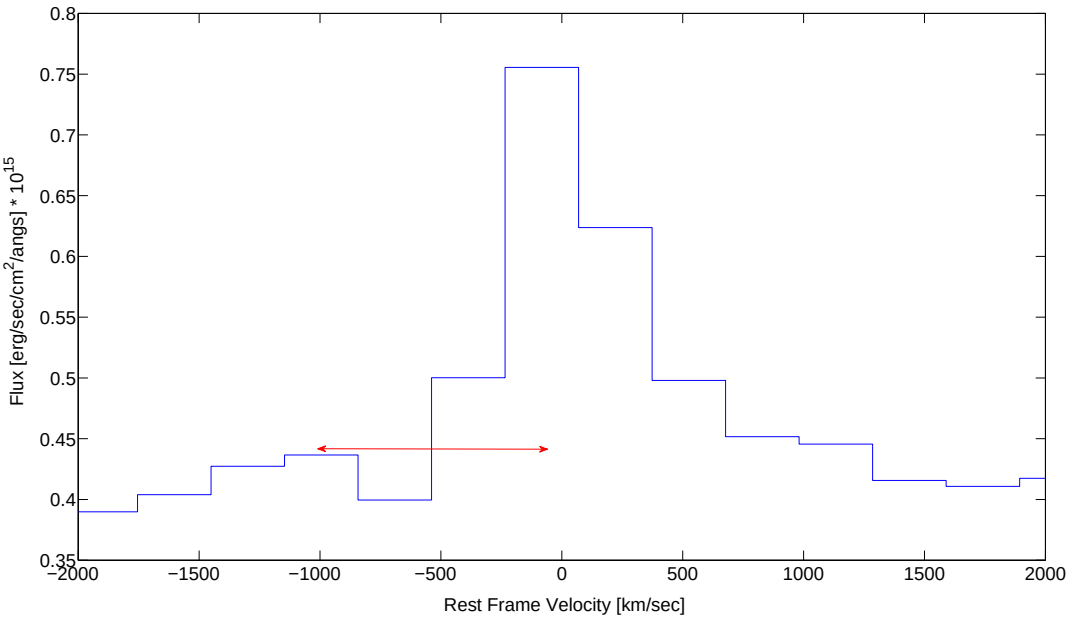

Fig. 12.— A Zoom-in on the H_β feature from a spectrum taken on September 8th, 2005, showing a narrow P-Cygni profile. The red arrow marks the velocity offset of the blue edge of the absorption feature.

3. Physical parameters of CCCP SNe IIn

3.1. Wind velocity calculation

We measured the widths of the intermediate and narrow components of the Hα emission line in our SN spectra and calculated the corresponding velocities using the Doppler formula. For each event the spectrum where the intermediate component was most evident was analyzed.

In order to measure the line widths, the H_α feature was decomposed using the following steps, implemented within *MATLAB*. First, the linear continuum surrounding of the line feature was removed. Next, a nonlinear least-squares script solved for the best-fit multi-Gaussian decomposition. Input parameters consisted of the number of components and an initial guess for the FWHM, height and center of each Gaussian, no other constraints were imposed. The scripts provide the user with the best-fit Gaussian width, height and center for each component as well as their corresponding errors. The errors are propagated into the wind velocity error. Line profile decompositions are shown in Figures 13 – 16. In all cases the best fits required both a narrow and an intermediate-width component. In some cases a broad component was also required. When appropriate, narrow P-Cygni profiles were smoothed. The measured velocities are reported in Table 4.

3.2. Mass loss rate calculation

The calculation is done via the following formula that relates the mass loss rate of the progenitor with the luminosity resulting from the ejecta-wind interaction (Chugai & Danziger 1994):

$$L_{H_\alpha} = \frac{1}{2}\epsilon_{H_\alpha}\dot{M}v_{shock}^2\frac{v_{shock}}{v_{wind}} \quad (1)$$

We assumed that the efficiency factor, $\epsilon_{H_\alpha} = 0.1$, appropriate for young SNe (Salamanca et al. 1998) and compatible with previous studies. v_{shock} is extracted from the intermediate component in the H_α feature (following the interpretation presented in section § 1; but see Chugai 2001; Dessart et al. 2009) and v_{wind} is extracted from the narrow component and/or the blue edge of the narrow P-Cygni profile (see below).

To derive the absolute H_α flux we performed synthetic photometry on the relevant spectra using the methods of Poznanski et al. (2002), compared the resulting R-band magnitude with our photometry (see above, interpolated as needed) and scaled the spectrum to match

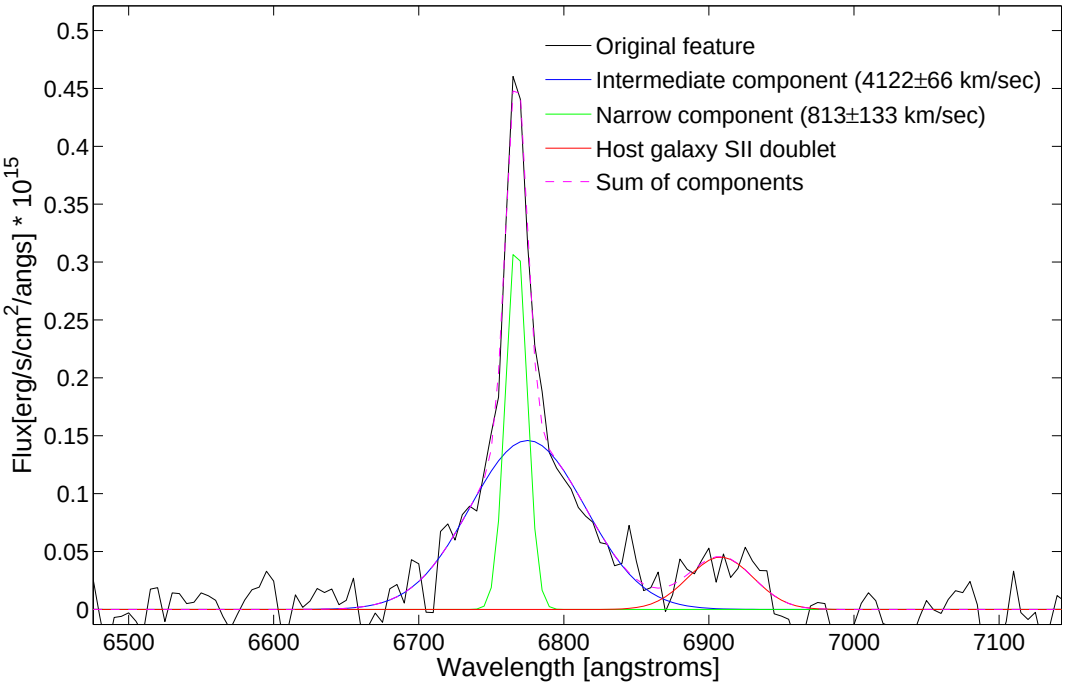

Fig. 13.— The decomposition of the H_α feature in the 30th of April 2005 spectrum of SN 2005bx.

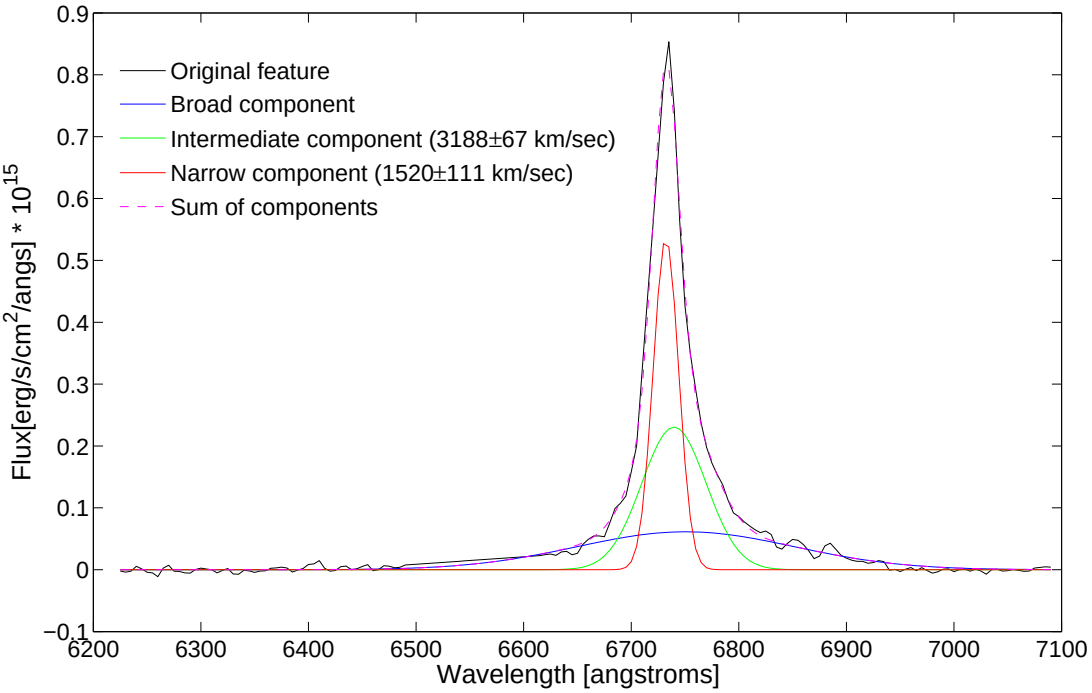

Fig. 14.— The decomposition of the H_α feature (post smoothing) in the 16th of July 2005 spectrum of SN 2005cl.

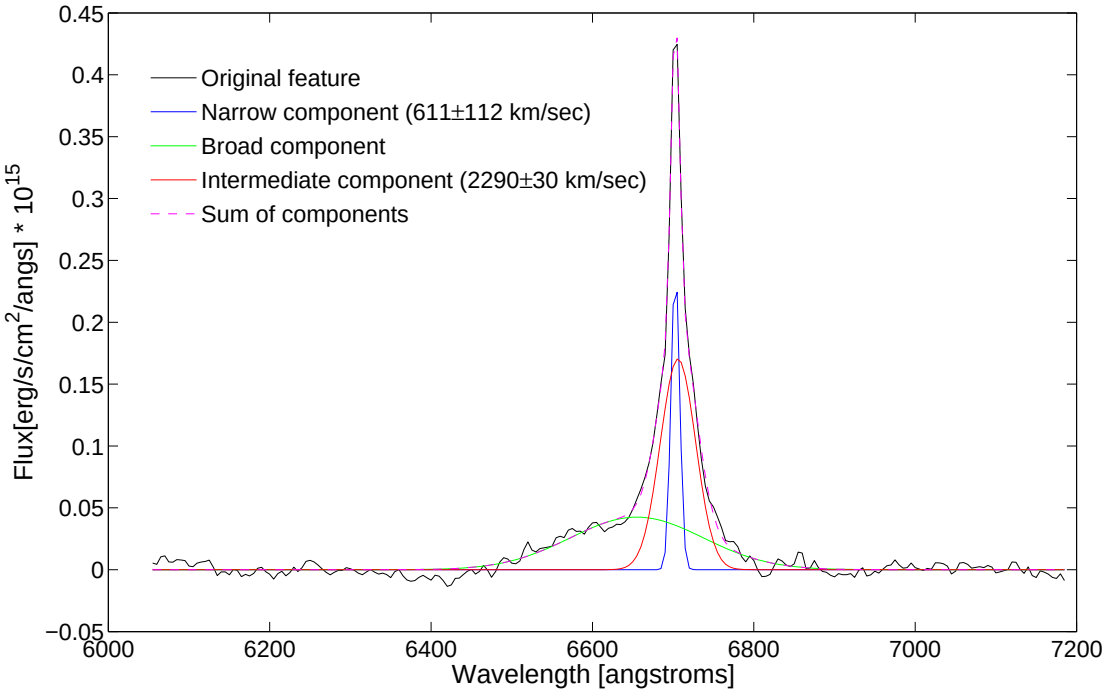

Fig. 15.— The decomposition of the H_α feature in the 13th of August 2005 spectrum of SN 2005cp.

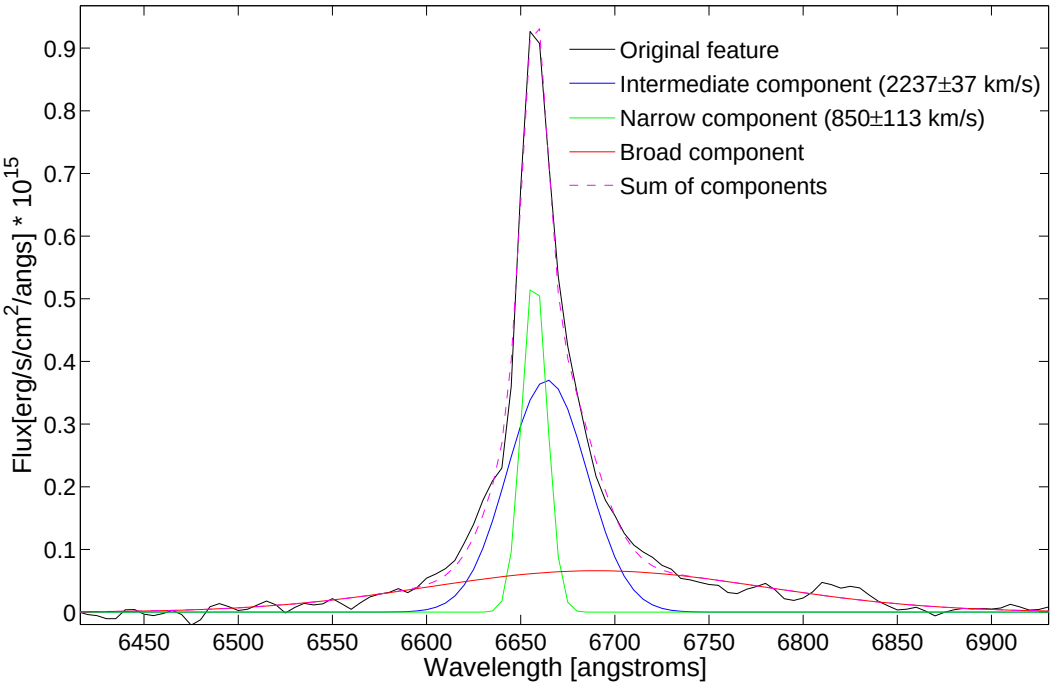

Fig. 16.— The decomposition of the H_α feature in the 14th of August 2005 spectrum of SN 2005db.

the absolute photometry. The resulting correction factors ranged between 1.7 and 3.2. The luminosity was then extracted by integrating over the intermediate-width-feature in the SN spectrum and accounting for the distance to the SN (obtained from NED). All measured values are reported in Table 4.

Following previous works, the shock velocity was taken as the FWHM of the intermediate-width component. The errors derived from the Gaussian decomposition of the H_α profile are provided by the least squares script output. Running the script with a different number of components (larger or smaller) turned out to provide poorer decompositions.

The unshocked wind velocity was derived from the HWZI of the narrow component. In addition to the error calculation procedure described above, the errors in the unshocked wind velocity also account for the uncertainty in the level of the continuum that translates to an uncertainty in the flux zero point when measuring the HWZI. All of the errors were propagated linearly into the velocity errors. The unshocked wind velocity was also calculated via the measurement of the P-Cygni profile, while taking the width as the difference between the H_α or H_β features peak and the blue edge of the absorption feature (Fig. 7, 10, 12). The errors of the P-Cygni velocities are calculated according our instrumental resolution, and the measured values are also corrected for the instrumental resolution – 4.88Å/pixel in the red band and 1.08Å/pixel in the blue band, following Alexander, Young & Hough (1999). These measurements are also reported in table 4.

For SN 2005cl and SN 2005cp, the unshocked-wind-velocity values used in the mass-loss-rate calculation include the range of values consistent with both the Gaussian fitting and the P-Cygni profile values. The average of the values in this range was taken as the unshocked wind velocity and the edges of this range determined the velocity error. For SN2005db, there was no overlap between the velocities derived by the two methods, so we considered the entire range of values defined by both methods (from the lower value of the Gaussian fitting to the top value of the P-Cygni profile). The final results can be seen in table 4.

The mass loss rates derived from Eq. 1 using the values derived above and their respective errors are reported in the final column of table 4.

Supernova	Shocked wind velocity [km s^{-1}]	unshocked wind velocity via Gaussian fitting [km s^{-1}]	unshocked wind velocity via P-Cygni profile [km s^{-1}]	unshocked wind velocity used for mass loss [km s^{-1}]	Mass loss rate [$M_\odot$ y^{-1}]
SN2005cl	3188 ± 67	1520 ± 111	1318 ± 223	1475 ± 65	0.12 ± 0.02
SN2005cp	2290 ± 30	611 ± 112	632 ± 225	610 ± 110	0.026 ± 0.005
SN2005db	2237 ± 37	850 ± 113	1113 ± 65	958 ± 220	0.057 ± 0.024
SN2005bx	4122 ± 66	813 ± 133	N/A	813 ± 133	0.037 ± 0.019

Table 4: Wind velocities and mass loss rates of SNe 2005bx, 2005cl, 2005cp, 2005db.

4. Previously studied SNe IIn

SNe IIn are rare. We have found only 15 SNe IIn for which progenitor mass-loss rates have been estimated in the literature, and few other events are discussed in detail (Table 5). For a single event (SN 2005gl) the progenitor was identified as a Luminous Blue Variable (LBV)-like star (Gal-Yam et al. 2007; Gal-Yam & Leonard. 2009) via pre-explosion images. SNe IIn exhibit a wide range of wind velocities and mass loss rates (tables 5).

In addition to conventional SNe IIn, there are other SNe that exhibit IIn characteristics. One group are the Ia/IIn Hybrids, also known as type IIa SNe (Deng et al. 2004). There is an argument whether these are explosions of white dwarfs interacting with circumstellar medium (Hamuy et al. 2003; Aldering et al. 2006) or the result of a core-collapse in massive stars (Benetti et al. 2006).

Another group that technically resembles SNe IIn are faint events that exhibit very narrow emission lines. These are often understood as LBV super-eruptions that leave the star intact (so-called "SN impostors") (Van Dyk 2006; Maund et al. 2006). We will not discuss these further here.

A review of literature events follows.

• SN 1987F is probably the first well-observed SN IIn, and thus predates the recognition of the class (and its definition) by Schlegel (1990). Spectroscopic observations were reported by Filippenko (1989) and Wegner & Swanson (1996). The event shows both narrow and intermediate-width components. The spectroscopic evolution of this object is quite similar to that of SN 2005cp in our sample (comparing Fig. 2 from Filippenko 1989 with our Fig 9). Photometric data have been presented by Filippenko (1989), Cappellaro et al. (1990), Wegner & Swanson (1996) and Tsvetkov (1989). The object was discovered after peak, but its reported magnitude ($M_V = -18.3\,\mathrm{mag}$; Filippenko 1989) is similar to that of SN 2005cp (and the average value of our CCCP sample), while the V-band decline rate reported by Cappellaro et al. (1990) and Wegner & Swanson (1996; $\sim 0.01\,\mathrm{mag\,day^{-1}}$) is also similar to that of SN 2005cp. Chugai (1991) derives a pre-explosion mass-loss rate using a formula similar to Eq. 1 of $\dot{M} = 10^{-3}\,\mathrm{M_\odot\,y^{-1}}$, assuming an unshocked wind velocity of $10\,\mathrm{km\,s^{-1}}$. Replacing this with the measured value of the narrow-line width from Wegner & Swanson (1996; $150\,\mathrm{km\,s^{-1}}$) would drive this value up to $\dot{M} \approx 10^{-2}\,\mathrm{M_\odot}$.

• SN 1988Z is the first extensively studied event, and is frequently mentioned in the literature. It was discovered post-maximum, and early photometric and spectroscopic observations are presented by Stathakis & Sadler (1991), Turatto et al. (1993a), Filippenko (1997) and Aretxaga et al. (1999). Chugai & Danziger (1994) estimate the pre-explosion mass loss rate to be between 7×10^{-4} and $1.5 \times 10^{-2}\,\mathrm{M_\odot\,y^{-1}}$.

• SN 1994W is a well-studied event discovered before maximum light and extensively followed. The general properties of this SN closely resemble our observations of SN 2005cl, with a similar spectral shape, absolute magnitude, rise and decline rates (Sollerman et al. 1998). These authors measure the unshocked wind velocity from the blue edge of the narrow P-Cygni profile to be $1000\,\mathrm{km\,s^{-1}}$. Chugai et al. (2004) present an extensive analysis of additional observations, and derive a very high mass-loss rate of $0.3\,\mathrm{M_\odot\,y^{-1}}$ using similar procedures to those we have employed. Interestingly, Dessart et al. (2009) have recently suggested that this event may have resulted from a collision between consecutive shells ejected by the progenitor, without the final core-collapse SN having occurred yet.

• SN 1994aj was studied by Benetti et al. (1998). Its spectra show some similarity to those of SN 2005cp, but its light curve decays significantly more rapidly ($\sim 0.4\,\mathrm{mag\,day^{-1}}$), though this decline rate slows down by factor of 10 or so at late times. Estimating the unshocked wind velocity to be $\sim 1000\,\mathrm{km\,s^{-1}}$ from the observed narrow P-Cygni profile and the shock velocity to be around $3700\,\mathrm{km\,s^{-1}}$ from the HWZI of the H_α emission line, these authors derive a mass-loss rate of $\sim 10^{-3}\,\mathrm{M_\odot\,y^{-1}}$, using Eq. 1.

• SN 1995G is another well-observed event. Pastorello et al. (2002) present extensive photometric and spectroscopic observations. Even though the peak was not observed, the data provided by these authors show this event appears to be similar to SN 2005cl in terms of its estimated peak magnitude ($\mathrm{M}_V = 18.5\,\mathrm{mag}$) and its initial decline rate ($\sim 0.01\,\mathrm{mag\,day^{-1}}$). At later times the decline slows down substantially. The spectra are similar to those of SN 2005cl presented above, including the blue continuum "bump" which is partially resolved into individual narrow P-Cygni profiles of numerous lines. Pastorello et al. (2002) estimate a moderate-mass rate ($\sim 2 \times 10^{-3}\,\mathrm{M_\odot\,y^{-1}}$) using Eq. 1. However, replacing their assumptions with values consistent with our methodology (efficiency ~ 0.1 and wind velocity estimated from the blue edge of the narrow P-Cygni profile, which would be $\sim 1200\,\mathrm{km\,s^{-1}}$ for this object), would drive the deduced mass-loss rate to very high values ($> 1\,\mathrm{M_\odot\,y^{-1}}$). Indeed, more sophisticated modeling of the same data set by Chugai & Danziger (2003) explains the properties of SN 1995G with an explosive mass ejection a few years before the supernova and leads to a mass-loss rate of $\sim 0.1\,\mathrm{M_\odot\,y^{-1}}$.

• SN 1995N occurred in a very nearby galaxy (24 Mpc), but was discovered long after explosion. Late-time optical and UV observations of SN 1995N are presented by Fransson et al. (2002). These authors measure the unshocked wind velocity to be $< 500\,\mathrm{km\,s^{-1}}$, and estimate the intermediate-width component velocity to be around $5000\,\mathrm{km\,s^{-1}}$, but do not estimate the mass loss rate of the progenitor. Zampieri et al. (2005) use X-ray data to estimate a mass-loss rate of $2 \times 10^{-4}\,\mathrm{M_\odot\,y^{-1}}$. Earlier observations verbally described by Baird et al. (1998) were apparently never published.

• SN 1996L is described by Benetti et al. (1999). Its light curve decays rapidly ($\sim 0.5\,\mathrm{mag\,day^{-1}}$), though this decline rate slows down by factor of 5 or so at late times. Observations began after maximum light, but these authors estimate a peak magnitude similar to that of SN 2005cp. Estimating the unshocked wind velocity to be $\sim 1600\,\mathrm{km\,s^{-1}}$ from the observed blue edge of the narrow P-Cygni profile and the average shock velocity to be around $4800\,\mathrm{km\,s^{-1}}$, these authors derive a mass-loss rate of $\sim 10^{-3}\,\mathrm{M_\odot\,y^{-1}}$, using Eq. 1.

• SN 1997ab was described by Hagen et al. (1997) and Salamanca et al. (1998). These authors use high-resolution spectroscopy to accurately measure the narrow P-Cygni profiles of the Balmer lines, and derive velocities of $90\,\mathrm{km\,s^{-1}}$ for the unshocked wind, and $\sim 6600\,\mathrm{km\,s^{-1}}$ for the shock. Using Eq. 1 they derive a mass-loss rate of $\sim 10^{-2}\,\mathrm{M_\odot\,y^{-1}}$.

• SN 1997eg was studied by Salamanca et al. (2002) spectroscopically. Photometric data are not reported. These authors identify a narrow P-Cygni profile in the Blamer lines, and use its blue edge to determine the unshocked wind velocity to be approximately $160\,\mathrm{km\,s^{-1}}$. Estimating the shock velocity to be $\sim 7000\,\mathrm{km\,s^{-1}}$, and using the same analysis used for SN 1997ab (and in out paper), they measure a mass-loss rate of $8.3 \times 10^{-3}\,\mathrm{M_\odot\,y^{-1}}$. Tsvetkov & Pavlyuk (2004) report a few photometric measurements of this event, while Hoffman et al. (2008) present a model for the star+CSM based on spectrophotometric and spectropolarimetric observations.

• SN 1998S is the most extensively observed SN IIn, and probably among the best-studied SN of any type. Nearby ($\sim$17 Mpc) and luminous, it was one of the brightest SNe of the last decades, and has been observed across the electromagnetic spectrum for many years. Early photometric and spectroscopic observations are reported by Liu et al. (2000), showing the SN peaked at $\mathrm{M}_B = -18.7$, broadly similar to the objects we studied. Its rise time ($< 20\,\mathrm{days}$) appears short compared to our sample of SNe IIn, and its decay is among the fastest ($\sim 0.05\,\mathrm{mag\,day^{-1}}$) measured for SNe IIn. Its early spectra resemble those of SN 2005cp (Fig. 9), in particular in the H_α profile and the broad lines on the blue side $1-2\,\mathrm{months}$ after peak. Additional spectroscopy is presented by Anupama et al. (2001), who derive a mass loss-rate of $10^{-4}\,\mathrm{M_\odot\,y^{-1}}$ assuming an unshocked wind velocity of $10\,\mathrm{km\,s^{-1}}$; we note that this value should be corrected upwards by a factor of a few given the wind velocities estimated by other authors from details analyses (e.g., $\mathrm{v}_w = 50\,\mathrm{km\,s^{-1}}$, Leonard et al. 2000; $\mathrm{v}_w = 30\,\mathrm{km\,s^{-1}}$ Bowen et al. 2000). The analysis of Lentz et al. (2001) using synthetic spectroscopy modeling indicates a mass-loss rate of $10^{-3} - 10^{-4}\,\mathrm{M_\odot\,y^{-1}}$ and wind speeds of $100 - 1000\,\mathrm{km\,s^{-1}}$. Analysis of the radio and X-ray observations of SN 1998S leads to similar estimates of the mass-loss rate (Pooley et al. 2002). Leonard et al. (2000) present an extensive spectroscopic and spectropolarimetric analysis, while Fassia et al. (2000, 2001) study large optical/IR photometric and spectroscopic data sets. Optical and UV *HST*

observations of SN 1998S are discussed by Bowen et al. (2000) and Fransson et al. (2005). The IR properties of this object are discussed by Gerardy et al. (2000) and Pozzo et al. (2004), and modeling of the spectroscopy is further discussed by Chugai (2001) and Chugai et al. (2002).

• SN 2005gl was studied by Gal-Yam et al. (2007) and Gal-Yam & Leonard (2009). This object appears to show a weaker interaction signature than other events discussed above, leading to a moderate peak magnitude (M~ -17 mag) and relatively fast decay ($\sim 0.04\,\mathrm{mag\,day^{-1}}$; Gal-Yam et al. 2007), as well a relatively rapid transition from an interaction-dominated spectrum to one similar to normal SNe II (Gal-Yam & Leonard 2009). Analysis by these authors using methods similar to those used in the current paper lead to estimates of the unshocked wind velocity $\mathrm{v}_w = 420\,\mathrm{km\,s^{-1}}$ (confirmed by Smith et al. 2010 using higher-resolution spectra); the shock velocity $\mathrm{v}_s = 1500\,\mathrm{km\,s^{-1}}$) and the mass-loss rate $0.03\,\mathrm{M_\odot\,y^{-1}}$. The analysis of Gal-Yam & Leonard provides strong evidence that the progenitor of this SN was a luminous LBV star.

• SN 2005ip was studied in detail by Smith et al. (2009). This object was not very luminous, with a peak magnitude of ~ -17.4 mag, and a relatively rapid decline ($\sim 0.02\,\mathrm{mag\,day^{-1}}$). The velocity of the unshocked wind is estimated to be $100-200\,\mathrm{km\,s^{-1}}$, and the shock velocity (measured from the intermediate-width component) is about $1100\,\mathrm{km\,s^{-1}}$. The mass-loss rate is estimated to be approximately $2\times10^{-4}\,\mathrm{M_\odot\,y^{-1}}$. The spectroscopic analysis supports suggestions concerning dust formation in the ejecta inferred from IR observations of this object by Fox et al. (2009).

• SN 2006gy attracted intensive attention due to its very high peak luminosity ($\mathrm{M}_V \sim -22$ mag), and it seems some late-time studies may still be going on, so a complete review of the literature may be premature. Early results were reported by Ofek et al. (2007), estimating a mass-loss rate of $0.1\,\mathrm{M_\odot\,y^{-1}}$, and Smith et al. (2007), who were more ambiguous about such high mass-loss values. Later analysis by Agnoletto et al. (2009), Smith et al. (2010) and Miller et al. (2010a) do seem to converge on a model invoking an extremely massive star experiencing strong CSM interaction. Smith et al. (2010) estimate the CSM velocity to be around $200\,\mathrm{km\,s^{-1}}$, the shock velocity to be around $4000\,\mathrm{km\,s^{-1}}$, and mass-loss rates on the order of $1\,\mathrm{M_\odot\,y^{-1}}$.

• SN 2006tf has been studied by Smith et al. (2008). This supernova experienced strong interaction with a very massive CSM, making the event very luminous (the object was caught already in decline, at $\mathrm{M}_R \approx -20.8$ mag). Assuming the unshocked CSM velocity at $\mathrm{v}_w = 190\,\mathrm{km\,s^{-1}}$ and the shock velocity at $\mathrm{v}_s = 2000\,\mathrm{km\,s^{-1}}$, these authors estimate very large mass-loss rates $0.1-0.2\,\mathrm{M_\odot\,y^{-1}}$ several decades prior to explosion, rising to $2.3-4.1\,\mathrm{M_\odot\,y^{-1}}$ a few years before the supernova.

• SN 2008iy was a remarkable event, with an unprecedented rise time of ~ 400 days, to its peak magnitude of $M_r = -19.1$ mag (Miller et al. 2010b). These authors measure the unshocked wind velocity to be $\sim 100\,\mathrm{km\,s^{-1}}$ (perhaps with components extending to $450\,\mathrm{km\,s^{-1}}$), and estimate the shock velocity to be around $5000\,\mathrm{km\,s^{-1}}$. They estimate the mass-loss rate in several ways, getting consistent results of $1 - 2 \times 10^{-2}\,\mathrm{M_\odot\,y^{-1}}$.

• A group of objects whose first well-studied member was SN 2002ic (Hamuy et al. 2003) have similarities with SNe IIn in that they show strong CSM interaction, but the nature of the inner explosion (thermonuclear explosion of a white-dwarf star or a core-collapse of a massive star) are still debated (e.g., Benetti et al. 2006; Trundle et al. 2008). Members tentatively included in this group are SN 1997cy (Germany et al. 2000; Turatto et al. 2000), SN 1999E (Rigon et al. 2003), SN 2002ic (e.g., Hamuy et al. 2003; Kotak et al. 2005) and SN 2005gj (Aldering et al. 2005; Trundle et al. 2008). Estimated mass-loss rates are within the same range seen for SNe IIn ($10^{-4} - 10^{-2}\,\mathrm{M_\odot\,y^{-1}}$; Kotak et al. 2004, Trundle et al. 2008).

• In addition to the objects listed above, several additional events are mentioned in the literature, on which little information is provided . These include SN 1978G (Schlegel 1990), SN 1978K (discovered long after explosion), SN 1984E (Gaskel 1984; Dopita et al. 1984 Henry & Branch 1987) SN 1987B (Schlegel 1990, Schlegel et al. 1996), SN 1987C (Schlegel 1990; Schlegel & Kirshner 1998), SN 1988I (Filippenko 1989), SN 1989C (Schlegel 1990; Turatto et al. 1993b), SN 1990S (Hamuy et al. 1993), SN 1994Y (Filippenko 1997; Ho et al. 2001; Tsvetkov & Pavlyuk 1997); SN 1994ak (Filippenko 1997); SN 1999el (Di Carlo et al. 2002); SN 2007rt (Trundle et al. 2009); SN 2003ma (Rest et al. 2009) and SN 2008fz (Drake et al. 2010). Some other recently reported events whose connection to SNe IIn is unclear are SN 2008es (Gezari et al. 2009; Miller et al. 2009) and SN 2007od (Andrews et al. 2010).

5. Discussion

5.1. Typical properties of SNe IIn

SNe IIn are rare, and the first few events noticed received some attention as peculiar type II SN. Following the high-profile work on SN 1988Z and the synthesis paper by Schlegel (1990), coining of the term SNe IIn, these objects became popular subjects of detailed papers throughout the next decade. This trend apparently died out with SN 1999el, and while the number of detected SNe IIn continued to rise, no detailed report on a SN IIn discovered between 1999 and 2003 was published. More recently, several SNe IIn have again

Supernova	Unshocked wind velocity [km s^{-1}]	Shocked wind velocity [km s^{-1}]	Mass loss rate rate [$M_\odot$ y^{-1}]	References
SN 1987F	150	6000	10^{-2}	[1] [2]
SN 1988Z	< 200	1200 - 1800	$7 \times 10^{-2} - 1.5 \times 10^{-2}$	[3] [4]
SN 1994W	1000	$\sim$4000	0.3	[5] [6]
SN 1994aj	1000	$\sim$3700	10^{-3}	[7]
SN 1995G	~ 1000	3000 - 4000	0.1	[8] [9] [10]
SN 1995N	< 500	2500 - 5000	2×10^{-4}	[11] [12]
SN 1996L	1600	4800	10^{-3}	[13]
SN 1997ab	90	6600	10^{-2}	[14]
SN 1997eg	160	7000	8.3×10^{-3}	[15]
SN 1998S	30-100	N/A	10^{-4} - 10^{-3}	[16] – [20]
SN 2005gl	420	1500	0.03	[21]
SN 2005ip	100 - 200	1100	2.2×10^{-4}	[22]
SN 2006gy	200	4000	0.1-1	[23] [24]
SN 2006tf	190	2000	0.1-4.1	[25]
SN 2008iy	100	5000	$1\text{-}2\times10^{-2}$	[26]

Table 5: Wind velocities, mass loss rates and references for SNe IIn in the literature. References: [1] Wegner & Swanson 1996; [2] Chugai 1991; [3] Stathakis & Sadler 1991; [4] Chugai & Danziger 1994; [5] Sollerman et al. 1998; [6] Chugai et al. 2004; [7] Benetti et al. 1998; [8] Pastorello et al. 2002; [9] this work; [10] Chugai & Danziger 2003; [11] Fransson et al. 2002; [12] Zampieri et al. 2005; [13] Benetti et al. 1999; [14] Salamanca et al. 1998; [15] Salamanca et al. 2002; [16] Anupama et al. 2001; [17] Bowen et al. 2000; [18] Leonard et al. 2000; [19] Lentz et al. 2001 ; [20] Pooley et al. 2002; [21] Gal-Yam & Leonard 2009; [22] Smith et al. 2009;[23] Ofek et al. 2007; [24] Smith et al. 2010; [25] Smith et al. 2008; [26] Miller et al. 2010

been reported, but each of these works was motivated by a conceived peculiarity or special property of its subject event (extreme luminosity, unusual spectral features, extended light curve, etc.). It thus seems that while the population of SNe IIn reported in earlier papers may be fairly representative of the observed population (but often poorly observed or discovered a long time after explosion), the latest papers (typically with better data) are of obviously non-representative events. It is in this context that the CCCP SNe IIn events are quite useful. Since the CCCP targeted every core-collapse SN by design, it likely describes more fairly the SN IIn population detected in nearby galaxies.

In Fig 17 we plot the absolute R-band light curves of every SN IIn detected before peak magnitude. As can be seen, the CCCP events provide a substantial increase to this small sample, and span the range of photometric properties in terms of peak magnitude of what could be viewed as the "normal" or "typical" population (i.e., excluding the recently-reported very luminous events that were singled out for publication for this reason).

In Fig. 18 we replot the light curve data normalized and shifted so that the peaks coincide. Our new CCCP data significantly increase the number of objects with well-measured rise times, especially if one focused on the "normal" luminosity range. We can see that SNe IIn typically have long rise times, up to 50 days, and diverse decline rates spanning the range from flat plateau events like SNe II-P to rapidly decaying events like SNe IIb. Since several events show obvious breaks or rapid changes in decline rates, the data suggest that extrapolating the light curves of SNe IIn discovered after explosion backwards in order to determine their peak magnitudes may not be a reliable procedure, and that one cannot assume a negligible rise time when estimating explosion dates from near-peak measurements.

Spectroscopically, our sample suggests that intermediate-width components and narrow P-Cygni profiles in the Balmer lines are ubiquitous among SNe IIn, and can usually be detected when a time-series of high-quality spectra is examined. Interestingly, combining our data with an extensive literature study, it seems like two spectroscopic groups of SNe IIn seem to manifest. The first, exemplified in our data by SN 2005cl, displays prominent narrow P-Cygni in the Balmer lines that persist with time, and a pointed, sharp profile of the H_{alpha} line. Other well studied members are SN 1994W and SN 1995G. On the other hand, some events, similar to SN 2005cp in our sample, show much weaker narrow P-Cygni profiles in the Balmer series that may only be visible for short periods of time, and have H_{alpha} line profiles that are triangular or boxy at late times. Other well-studied members include SN 1987F, SN 1994aj and SN 1998S. A more complete investigation of the physical reality and nature of this division lies beyond the scope of this work.

Finally, it is interesting to note that only one out of the four events we studied (with similar data) shows a partially resolved pseudo-continuum in the blue (Fig. 8; see Smith

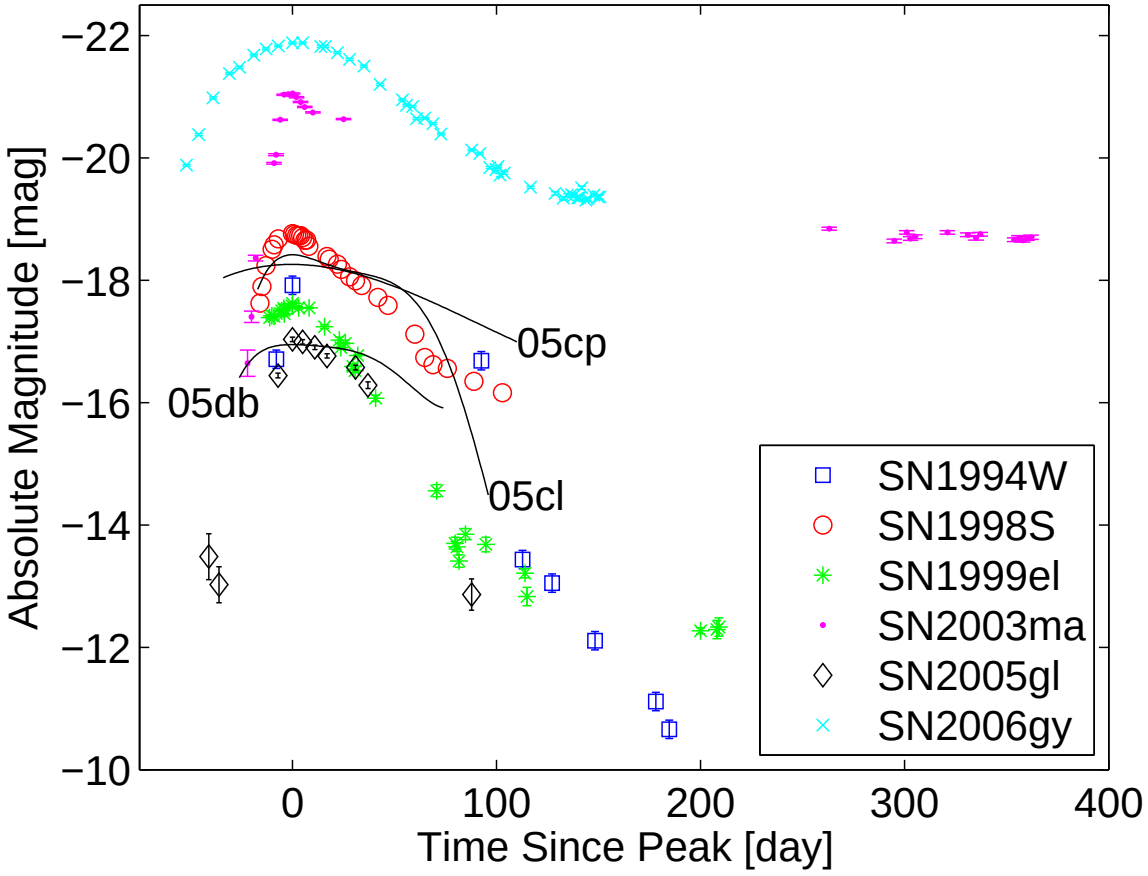

Fig. 17.— R-band absolute magnitudes of SNe IIn from the literature and from this work. The figure includes every SN IIn for which photometry covering the peak is available in the literature (see references in § 4). The CCCP events are displayed as smooth curves (see 2.2) and span the range of photometric properties of "normal" SNe IIn in terms of peak magnitude ($M_R = -17 - 18.5$), but appear to have more extended light curves.

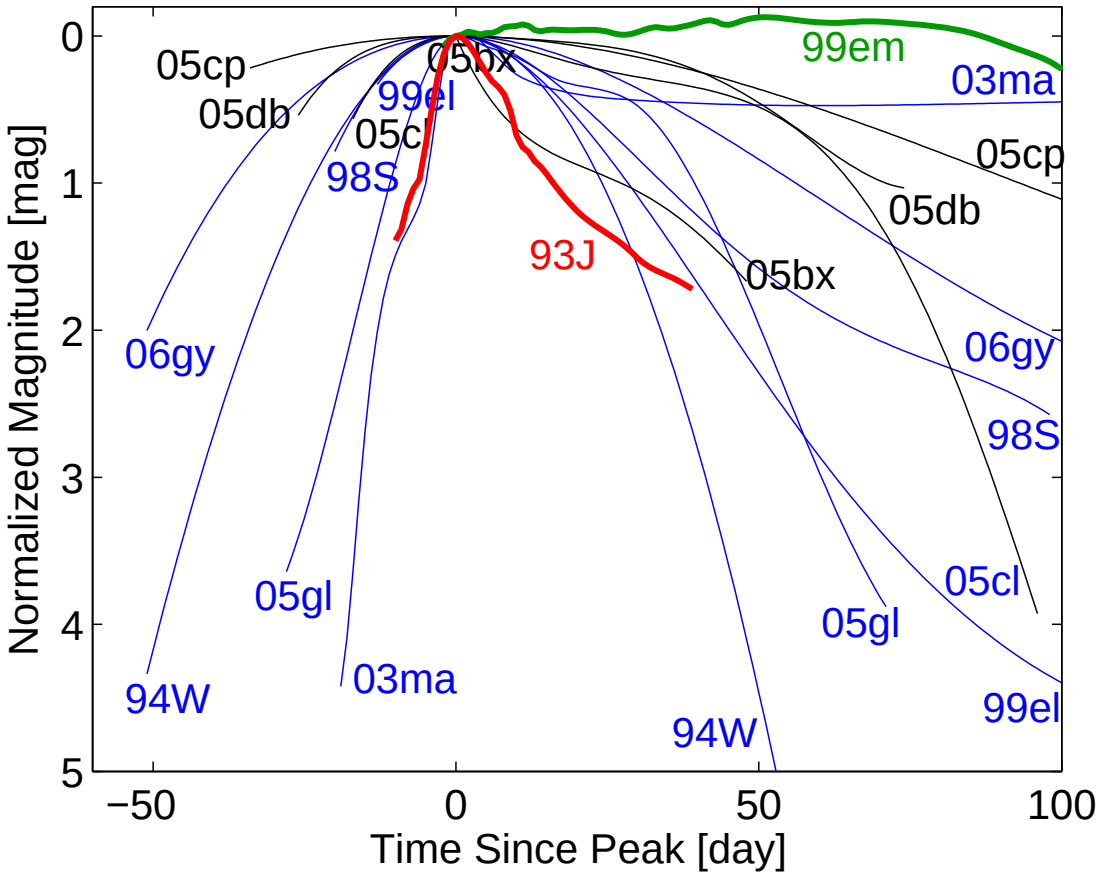

Fig. 18.— The data in Fig. 17 normalized to have the same peak magnitude and shifted in time so the peaks coincide. We overplot for comparison the light curves of the prototypical type II-P SN 1999em, and the rapidly declining type IIb SN 1993J. One can see that the decline rates of SNe IIn span the range between these two extremes. On the other hand, the rise times of SNe IIn are typically long, extending up to 50 days or more. These data indicate that estimates of explosion dates and peak magnitudes derived for SNe IIn discovered in the decline phase are not reliable, as rise times can be long and decline rates vary substantially.

et al. 2009 for a recent discussion). It is not clear yet if all SNe IIn have blue pseudo-continuum dominated by blended Fe-group lines, which is only resolved in a few cases, or if this phenomenon is rare. It is interesting to note that beside being the only event showing a resolved pseudo continuum, SN 2005cl is also the SN with the fastest pre-explosion wind velocity and largest mass-loss value in our sample. A systematic study of a larger sample of SNe IIn may also shed light on this aspect.

5.2. Implications for the progenitor stars

The mass loss rates we derive for the CCCP SNe IIn in this work are indicative of progenitor stars with LBV-like behavior, as our values (few 10^{-2} to $0.12\,M_{\odot}\,y^{-1}$) are essentially too high for any class of massive stars other than LBVs in the eruptive phase (Humphreys & Davidson 1994). All events also exhibit high wind velocities, that is some cases ($1475 \pm 65\,km\,s^{-1}$ for SN 2005cl) are quite extreme compared with most known LBVs (though see the recent measurements by Pastorello et al. 2010 for a counter example). Thus, it is quite possible that the properties of massive stars shortly before they explode do not resemble these of stars seen in our galaxy that have not yet reached these late, short-lived stages. While the luminous progenitor of SN 2005gl (Gal-Yam & Leonard 2009) and very high deduced mass-loss rates of some SNe (e.g., SN 2006gy, Smith et al. 2009; SN 2006tf, Smith et al. 2008) suggest that some SNe IIn come from extremely massive stars, it is not clear if this is true for all these events. In this context, our measurements of high mass-loss rates argue against the progenitors of SNe IIn being red giant stars, whose wind velocities and mass-loss rates are too low, and the strong hydrogen lines and extended light curves argue against Wolf-Rayet stars, whose atmospheres are expected to be hydrogen-poor and compact (some W-R stars may explain the class of interacting H-poor Ibn SNe; Pastorello et al. 2008). Thus it seems that SNe IIn as a class (if all or most of the objects arise from a single group of massive stars) require a progenitor star that does not fit any of the common classes of massive stars. Such rare progenitor stars are naturally explained by extreme masses, though other explanations are possible.

6. Summary and conclusions

SNe IIn exhibit a wide range of wind velocities and mass loss rates (tables 5). We have presented our observations of four representative SNe IIn observed by the CCCP project. Our photometry allows to determine peak magnitudes, rise and decline rates for three events. Our spectroscopic time series are used to measure the pre-explosion wind velocities and mass-

loss rates from the progenitor stars of these SNe. We then provide an extensive review of the literature and discuss our results in the context of other well-studied events. Our main results are:

• SNe IIn are typically luminous compared to other core-collapse SNe (peak $M_V = -18.4\,\mathrm{mag}$), and have a relatively long rise time ($> 20\,\mathrm{days}$) followed by a slow decline.

• SN IIn spectra often show prominent narrow P-Cygni profiles in the Balmer lines, and multi-component H_{alpha} profiles.

• We measure fast pre-explosion progenitor winds ($600 - 1400\,\mathrm{km\,s^{-1}}$) and derive large mass-loss rates ($0.026 - 0.12\,\mathrm{M_\odot\,y^{-1}}$).

• Our work supports the association between type IIn SNe and LBV-like progenitor stars. The strong and massive winds we find are broadly consistent with LBV progenitor stars and unlike those of typical red supergiants. This is in accordance with the only well observed IIn SN case where pre-explosion images of the progenitor were taken (Gal-Yam & Leonard. 2009).

7. Acknowledgments

We thank N. Chugai, A. Pastorello, S. Benetti and N. Smith for useful comments on the manuscript. The work of A. G. is supported by grants from the Israeli Science Foundation (ISF), an EU FP7 Marie Curie IRG fellowship, the Benoziyo Cenetr for Astrophysics and a research grant from the Peter and Patricia Gruber Awards. S.B.C. acknowledges generous support from Gary and Cynthia Bengier and the Richard and Rhoda Goldman fund.

REFERENCES

Abbott, D. C., & Conti, P. S. 1987, ARA&A, 25, 113

Agnoletto, I., et al. 2009, ApJ, 691, 1348

Aldering, G., et al. 2006, ApJ, 650, 510

Andrews, J. E., et al. 2010, ApJ, 715, 541

Anupama, G. C., Sivarani, T., & Pandey, G. 2001, A&A, 367, 506

Aretxaga, I., Benetti, S., Terlevich, R. J., Fabian, A. C., Cappellaro, E., Turatto, M., & della Valle, M. 1999, MNRAS, 309, 343

Arnett, W. D., Bahcall, J. N., Kirshner, R. P., & Woosley, S. E. 1989, ARA&A, 27, 629

Baird, M. D., Garnavich, P. M., Schlegel, E. M., Challis, P. M., & Kirshner, R. P. 1998, Bulletin of the American Astronomical Society, 30, 1323

Benetti, S., Cappellaro, E., Danziger, I. J., Turatto, M., Patat, F., & della Valle, M. 1998, MNRAS, 294, 448

Benetti, S., Turatto, M., Cappellaro, E., Danziger, I. J., & Mazzali, P. A. 1999, MNRAS, 305, 811

Benetti, S., Cappellaro, E., Turatto, M., Taubenberger, S., Harutyunyan, A., & Valenti, S. 2006, ApJ, 653, L129

Bertin, E., & Arnouts, S. 1996, A&AS, 117, 393

Bessell, M. S. 1999, PASP, 111, 1426

Blanc, N., et al. 2005, The Astronomer's Telegram, 570, 1

Bonnaud, C., et al. 2005, The Astronomer's Telegram, 474, 1

Bowen, D. V., Roth, K. C., Meyer, D. M., & Blades, J. C. 2000, ApJ, 536, 225

Cappellaro, E., della Valle, M., Iijima, T., & Turatto, M. 1990, A&A, 228, 61

Cenko, S. B., et al. 2006, PASP, 118, 1396

Chugai, N. N. 1991, MNRAS, 250, 513

Chugai, N. N., & Danziger, I. J. 1994, MNRAS, 268, 173

Chugai, N. N. 2001, MNRAS, 326, 1448

Chugai, N. N., Blinnikov, S. I., Fassia, A., Lundqvist, P., Meikle, W. P. S., & Sorokina, E. I. 2002, MNRAS, 330, 473

Chugai, N. N., & Danziger, I. J. 2003, Astronomy Letters, 29, 649

Chugai, N. N., et al. 2004, MNRAS, 352, 1213

Deng, J., et al. 2004, ApJ, 605, L37

Dessart, L., Hillier, D. J., Gezari, S., Basa, S., & Matheson, T. 2009, MNRAS, 394, 21

Di Carlo, E., et al. 2002, ApJ, 573, 144

Dopita, M. A., Cohen, M., Schwartz, R. D., & Evans, R. 1984, ApJ, 287, L69

Drake, A. J., et al. 2010, ApJ, 718, L127

Fassia, A., et al. 2000, MNRAS, 318, 1093

Fassia, A., et al. 2001, MNRAS, 325, 907

Filippenko, A. V. 1989, AJ, 97, 726

Filippenko, A. V. 1997, ARA&A, 35, 309

Filippenko, A. V., Li, W. D., Treffers, R. R., & Modjaz, M. 2001, IAU Colloq. 183: Small Telescope Astronomy on Global Scales, 246, 121

Fox, O., et al. 2009, ApJ, 691, 650

Fransson, C., et al. 2002, ApJ, 572, 350

Fransson, C., et al. 2005, ApJ, 622, 991

Gal-Yam, A., et al. 2004, ApJ, 609, L59

Gal-Yam, A., Sand, D. J., Cenko, S. B., Leonard, D. C., & Muller, J. 2005, The Astronomer's Telegram, 475, 1

Gal-Yam, A., et al. 2007, ApJ, 656, 372

Gal-Yam, A., Cenko, S. B., Fox, D. B., Leonard, D. C., Moon, D.-S., Sand, D. J., & Soderberg, A. M. 2007, The Multicolored Landscape of Compact Objects and Their Explosive Origins, 924, 297

Gal-Yam, A., Maoz, D., Guhathakurta, P., & Filippenko, A. V. 2008, ApJ, 680, 550

Gal-Yam, A., & Leonard, D. C. 2009, Nature, 458, 865

Gaskel, C. M. 1984, PASP, 96, 789

Gerardy, C. L., Fesen, R. A., Höflich, P., & Wheeler, J. C. 2000, AJ, 119, 2968

Germany, L. M., Reiss, D. J., Sadler, E. M., Schmidt, B. P., & Stubbs, C. W. 2000, ApJ, 533, 320

Gezari, S., et al. 2009, ApJ, 690, 1313

Hagen, H.-J., Engels, D., & Reimers, D. 1997, A&A, 324, L29

Hamuy, M., et al. 1993, AJ, 106, 2392

Hamuy, M., et al. 2003, Nature, 424, 651

Henry, R. B. C., & Branch, D. 1987, PASP, 99, 112

Ho, W. C. G., Van Dyk, S. D., Peng, C. Y., Filippenko, A. V., Leonard, D. C., Matheson, T., Treffers, R. R., & Richmond, M. W. 2001, PASP, 113, 1349

Hoffman, J. L., Leonard, D. C., Chornock, R., Filippenko, A. V., Barth, A. J., & Matheson, T. 2008, ApJ, 688, 1186

Horne, K. 1986, PASP, 98, 609

Humphreys, R. M., & Davidson, K. 1994, PASP, 106, 1025

Jordi, K., Grebel, E. K., & Ammon, K. 2005, Astronomische Nachrichten, 326, 657

Kinney, A. L., Calzetti, D., Bohlin, R. C., McQuade, K., Storchi-Bergmann, T., & Schmitt, H. R. 1996, ApJ, 467, 38

Kotak, R., Meikle, W. P. S., Adamson, A., & Leggett, S. K. 2004, MNRAS, 354, L13

Lee, E., Ponticello, N. J., & Li, W. 2005, IAU Circ., 8550, 1

Lentz, E. J., et al. 2001, ApJ, 547, 406

Leonard, D. C., Filippenko, A. V., Barth, A. J., & Matheson, T. 2000, ApJ, 536, 239

Liu, Q.-Z., Hu, J.-Y., Hang, H.-R., Qiu, Y.-L., Zhu, Z.-X., & Qiao, Q.-Y. 2000, A&AS, 144, 219

Matheson, T., Filippenko, A. V., Ho, L. C., Barth, A. J., & Leonard, D. C. 2000, AJ, 120, 1499

Maund, J. R., et al. 2006, MNRAS, 369, 390

Miller, A. A., et al. 2009, ApJ, 690, 1303

Miller, A. A., Smith, N., Li, W., Bloom, J. S., Chornock, R., Filippenko, A. V., & Prochaska, J. X. 2010a, AJ, 139, 2218

Miller, A. A., et al. 2010b, MNRAS, 404, 305

Minkowski, R. 1941, PASP, 53, 224

Modjaz, M., Kirshner, R., Challis, P., & Berlind, P. 2005, IAU Circ., 8544, 4

Modjaz, M., Kirshner, R., Challis, P., & Hutchins, R. 2005, IAU Circ., 8557, 3

Monard, L. A. G. 2005, IAU Circ., 8571, 1

Ofek, E. O., et al. 2007, ApJ, 659, L13

Oke, J. B., & Gunn, J. E. 1982, PASP, 94, 586

Pastorello, A., et al. 2002, MNRAS, 333, 27

Pastorello, A., et al. 2008, MNRAS, 389, 113

Pastorello, A., et al. 2010, MNRAS, 408, 181

Pooley, D., et al. 2002, ApJ, 572, 932

Pozzo, M., Meikle, W. P. S., Fassia, A., Geballe, T., Lundqvist, P., Chugai, N. N., & Sollerman, J. 2004, MNRAS, 352, 457

Pugh, H., & Li, W. 2005, IAU Circ., 8544, 3

Rest, A., et al. 2009, arXiv:0911.2002

Rich, D. 2005, IAU Circ., 8521, 1

Rigon, L., et al. 2003, MNRAS, 340, 191

Salamanca, I., Cid-Fernandes, R., Tenorio-Tagle, G., Telles, E., Terlevich, R. J., & Munoz-Tunon, C. 1998, MNRAS, 300, L17

Salamanca, I., Terlevich, R. J., & Tenorio-Tagle, G. 2002, MNRAS, 330, 844

Schlegel, E. M. 1990, MNRAS, 244, 269

Schlegel, E. M., Kirshner, R. P., Huchra, J. P., & Schild, R. E. 1996, AJ, 111, 2038

Schlegel, D. J., Finkbeiner, D. P., & Davis, M. 1998, ApJ, 500, 525

Schlegel, E. M., & Kirshner, R. P. 1998, New Astronomy, 3, 125

Smartt, S. J. 2009, ARA&A, 47, 63

Smith, N., et al. 2007, ApJ, 666, 1116

Smith, N., Chornock, R., Li, W., Ganeshalingam, M., Silverman, J. M., Foley, R. J., Filippenko, A. V., & Barth, A. J. 2008, ApJ, 686, 467

Smith, N., et al. 2009, ApJ, 695, 1334

Smith, N., Chornock, R., Silverman, J. M., Filippenko, A. V., & Foley, R. J. 2010, ApJ, 709, 856

Sollerman, J., Cumming, R. J., & Lundqvist, P. 1998, ApJ, 493, 933

Stathakis, R. A., & Sadler, E. M. 1991, MNRAS, 250, 786

Trundle, C., Kotak, R., Vink, J. S., & Meikle, W. P. S. 2008, A&A, 483, L47

Trundle, C., et al. 2009, A&A, 504, 945

Tsvetkov, D. Y. 1989, Soviet Astronomy Letters, 15, 129

Tsvetkov, D. Y., & Pavlyuk, N. N. 1997, Astronomy Letters, 23, 26

Tsvetkov, D. Y., & Pavlyuk, N. N. 2004, Astronomy Letters, 30, 32

Turatto, M., Cappellaro, E., Danziger, I. J., Benetti, S., Gouiffes, C., & della Valle, M. 1993a, MNRAS, 262, 128

Turatto, M., Cappellaro, E., Benetti, S., & Danziger, I. J. 1993b, MNRAS, 265, 471

Turatto, M., et al. 2000, ApJ, 534, L57

Turatto, M., Benetti, S., & Cappellaro, E. 2003, From Twilight to Highlight: The Physics of Supernovae, 200

van Dyk, S. D. 2006, Calibrating the Top of the Stellar M-L Relation, 26th meeting of the IAU, Joint Discussion 5, 16 August 2006, Prague, Czech Republic, JD05, #6, 5,

Wade, R. A., & Horne, K. 1988, ApJ, 324, 411

Wegner, G., & Swanson, S. R. 1996, MNRAS, 278, 22

Zampieri, L., Mucciarelli, P., Pastorello, A., Turatto, M., Cappellaro, E., & Benetti, S. 2005, MNRAS, 364, 1419

Appendix: photometric calibration

In Fig. 19 we show finding charts for the SNe and nearby calibration stars, whose magnitudes are given in table 7.

	Star	RA	Dec	B	V	R	I
SN2005bx	1	13:50:36.5	+68:35:23.0	17.18	16.15	15.64	15.17
	2	13:50:54.7	+68:33:27.0	18.06	16.72	15.99	15.35
	3	13:50:33.2	+68:32:48.3	14.76	14.07	13.63	13.26
SN2005cl	1	21:02:07.4	-06:17:12.5	18.54	17.97	17.65	17.26
	2	21:02:08.6	-06:18:30.4	18.05	17.29	16.84	16.38
	3	21:02:05.0	-06:19.09.4	15.50	14.64	14.02	13.85
	4	21:02:03.8	-06:19:38.2	15.91	15.12	14.58	14.34
	5	21:02:18.4	-06:19:57.2	14.97	14.07	13.60	13.21
SN2005cp	1	23:59:44.2	+18:10:42.2	15.03	14.28	13.83	13.44
	2	23:59:54.2	+18:08:23.3	17.09	16.05	15.43	14.92
	3	23:59:42.1	+18:07:51.5	18.09	17.52	17.12	16.65
SN2005db	1	00:41:26.0	+25:32:40.6	15.32	14.46	13.99	13.53
	2	00:41:26.2	+25:31:57.4	16.44	15.87	15.56	15.22
	3	00:41:20.9	+25:29:12.5	18.13	17.11	16.53	15.98
	4	00:41:24.1	+25:28:21.2	16.88	16.24	15.89	15.50

8. SDSS vs. Landolt calibrations

Landolt-derived equations for the observing nights of 2005 August 31 and 2009 April 19 were used to calibrate 15 stars located near 4 CCCP SNe within the SDSS footprint. The standard Landolt results were compared with magnitudes obtained from the SDSS photometry of these stars as above. The difference between the two calibrations was calculated in each filter for each star as well as the average and the standard deviation of the differences of all the stars. The results from both nights are shown in table 8.

In all the filters, the scatter in the differences is larger than the mean offsets. We conclude that the two calibration methods are consistent.

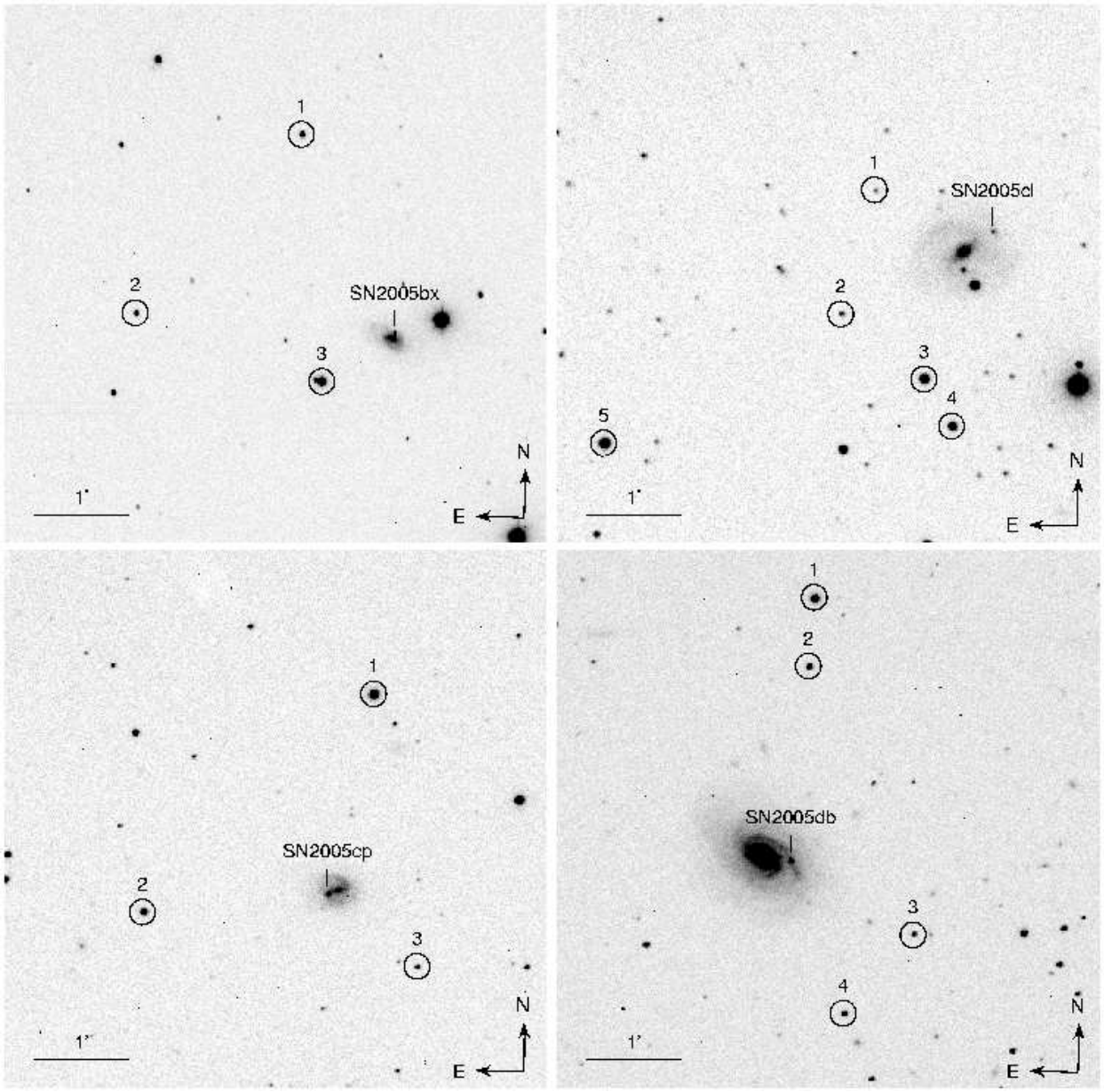

Fig. 19.— Calibration stars in the fields of the SNe studied in this paper. The SNe are marked by tick marks, stars are circled and numbered (matching table 7). North is up, East is due left, a scale bar is provided.

	20050831				20090419			
	B	V	R	I	B	V	R	I
Average magnitude difference	0.014	-0.004	0.019	0.021	0.016	0.051	0.040	0.007
Standard deviation	0.076	0.021	0.045	0.048	0.109	0.080	0.049	0.025

Table 6: Comparison between SDSS calibration and Landolt calibrations.